This is to certify that the
thesis entitled

THE DESIGN AND OPTIMIZATION OF AN AUTOMOBILE COOLING FAN

presented by

EMMETT DEMPSEY

has been accepted towards fulfillment
of the requirements for the

M.S. degree in MECHANICAL ENGINEERING

Major Professor's Signature

08/25/06

Date

THE DESIGN AND OPTIMIZATION OF AN AUTOMOBILE COOLING FAN

By

Emmett Dempsey

A THESIS

Submitted to
Michigan State University
in partial fulfillment of the requirements
for the degree of

MASTER OF SCIENCE

Department of Mechanical Engineering

2006

ABSTRACT

THE DESIGN AND OPTIMIZATION OF AN AUTOMOBILE COOLING FAN

By Emmett Dempsey

The goal of this investigation was to design a fan for automotive cooling applications. Modern automobiles have several heat exchangers within the engine compartment that are stacked together to form the radiator. A cooling fan was required to produce a sufficient, uniform cooling flow of air through the stack, having high efficiency, low weight and cost, and optimum mechanical properties in a high temperature (393 K) environment. Given the inlet conditions, an initial 1-D design was performed. 2-D blade contours were then designed using the inverse design method and an inviscid flow assumption. The 2-D inviscid designs were then analyzed using Navier-Stokes software. 3-D meshes were created by stacking the 2-D blade contours and analyzed using two software packages: TRAF3D and CFX. To improve the performance of each blade, a 3D optimization was performed using the TRAF3D Navier-Stokes software and the addition of circumferential lean.

ACKNOWLEDGEMENTS

Firstly, I would like to thank my professors Dr. Mueller and Dr. Engeda in the mechanical engineering department at Michigan State University. Not only have they provided me with academic guidance, but also with several opportunities to expand my personal horizons, including co-authoring conference papers and studying at the Von Karman Institute in Belgium.

I would also like to thank Prof. Van den Braembussche at the Von Karman Institute for his wise guidance and supervision on the compressor design project. Dr. Z. Alsalihi, J. Prinsier, and T. Verstraete also provided me with all of the technical assistance and advice necessary to complete the project. I could not have made such a smooth transition to the available computer operating systems or understand the software without their help.

My friends at the VKI, especially Giorgio, Javi, and Marco made my time at the VKI very enjoyable and an experience that I will never forget. Although I am happy to be finishing the diploma course, I wish that my time with them would never end. They became my European family.

Finally, I would like to thank my family and friends in Michigan for all of the encouragement they have given me. From encouraging me to study at Michigan State University to supporting me in Belgium, they have always been here for me.

TABLE OF CONTENTS

LIST OF TABLES

LIST OF FIGURES

LIST OF SYMBOLS

c.....Chord (meters)

f.....Vertex Angle of Triangle r-z-y (degrees)

m.....Mass Flow Rate (kilograms per second)

r.....radius (meters)

t.....Pitch (meters)

x.....Axial Coordinate (meters)

y.....Circumferential Coordinate (meters)

z.....Radial Coordinate (meters)

H.....Enthalpy (Joules per kilogram)

P.....Pressure (Pascals)

T.....Temperature (Kelvin)

U.....Rotational Velocity (meters per second)

V.....Velocity in Absolute System (meters per second)

W.....Velocity in Relative System (meters per second)

Z.....Number of Blades

α.....Flow Angle in Absolute System (degrees)

β.....Flow Angle in Relative System (degrees)

η.....Polytropic Compression Efficiency (unitless)

λ.....Stagger Angle (degrees)

ρ.....Density (kilograms per cubic meter)

s.....Solidity (unitless)

ω.....Rotational Speed (revolutions per minute)

subscripts

ax.....Axial Component

hub.....Hub Blade Section

is.....Isentropic

mid.....Middle Blade Section

tan.....Tangential Component

tip.....Tip Blade Section

S.....Static Quantity

0.....Total Quantity

1.....Inlet Station, Upstream of the Blade

2.....Exit Station, Downstream of the Blade

THE DESIGN AND OPTIMIZATION OF AN AUTOMOBILE COOLING FAN

4.1 Introduction

Automobile engines produce heat from several different sources, including internal combustion and friction of the moving parts. Cooling fluids are necessary to remove the heat from the engine block, air conditioning system, engine oil, and turbocharger, and maintain a sufficiently low operating temperature for both the engine and passengers. The cooling fluids pass through a radiator stack where the heat is exchanged with ambient air. In order to provide the cooling flow through the radiator stack, a fan is required. Besides the basic pressure rise and mass flow requirements, the fan also needs to have high efficiency, low weight and cost, good mechanical properties in the operating conditions, long life, and provide a uniform flow. The goal of this project was to design a fan to meet all of these requirements.

The design process consisted of several important steps. The first step was to create an initial 1-Dimensional design based on the given thermodynamic requirements. This step yielded the flow velocities and angles necessary for the 2-Dimensional design. In the second step, a 2-Dimensional, inviscid blade contour was designed using the inverse design method at three different radial locations on the fan blade. A viscous 2-Dimensional analysis was then performed and compared to the inviscid results. The contours were then stacked into a complete blade and analyzed with a 3-Dimensional Navier-Stokes flow solver. To validate these results, the results from another flow solver were employed. Next, the 3-Dimensional blade shape was optimized aerodynamically and mechanically with the addition of circumferential lean. Finally, the performance space for the optimized blade was determined. Similar work has been done by K. K.

Pehlivan[1], who redesigned a fan using the inverse design method and performed a CFX analysis of the original blade design.

4.2 Method

4.2.1 1-Dimensional Design

The goal of the 1-D design was to determine from the specified data what the inlet and outlet flow velocities and angles are required to be for the single-stage, shrouded fan without inlet guide vanes. The requirements provided by Valeo[2] are shown in Table 1. Knowing these values and using air as the working fluid, all geometrical values were determined using equations 7-10 in Appendix 5c. By assuming a polytropic compression efficiency of $\eta = 0.7$ and using the thermodynamic equations 11-13, the outlet flow angles were determined. Inlet flow angles were calculated knowing the RPM, radius, and inlet flow. Therefore, the total flow turning ($\Delta\beta$) from inlet to outlet was known, as were the absolute and relative velocities at inlet and outlet.

Initially, there was a design philosophy for constant static pressure rise across the blade. This proved impractical, because no amount of turning at the hub section could produce the necessary pressure rise for the given rotational speed. As seen in Table 2, the maximum pressure rise attainable at the hub section is 187.8 Pa at a flow turning of 70.22 degrees. Also, the tip required only 1.08 degrees of turning to achieve the necessary pressure rise. This can be attributed to the larger radius at the tip section than the hub section. In other words, the tip section work is done mostly by the rotational U velocity component while the hub section work requires more $\Delta\beta$ to do the same amount of work (see equation 11). To make up for the lack of pressure rise at the hub section, the middle

and tip sections were designed for more pressure rise, while the hub section was unloaded slightly to reduce the turning. The actual blade data can be seen in Table 3.

4.2.2 2-Dimensional Design

The purpose of creating the 2-D blade contour designs at three different radii (hub, middle, and tip) was to create a basic frame from which the complete, 3-D blade would be created. The 2-D design method implemented was an inverse, inviscid method. Unlike the traditional design method, the inverse design method involves starting with a prescribed velocity distribution on suction and pressure sides and computing a 2-D blade contour geometry. The programs used were INVC, INVCPL and INVC-MOD. INVC-MOD was used to modify either the actual or required velocity distribution. INVC was used to analyze (1 iteration) or converge (multiple iterations) to the required velocity distribution. INVCPL was used to visualize the blade contour and velocity distribution.

The INVC code required an initial blade geometry as a base design, which theoretically could have been any blade. A NACA65 blade was chosen to start with due to its already favorable characteristics. Input parameters included t/c, λ, and β_1. After an initial analysis of the blade, a velocity file was automatically created. The velocity at discrete points along the blade chord for both pressure and suction side were stored in this file for independent modification using INVC-MOD. After modification, a required velocity file was created, and INVC was used to determine the physical blade shape for the required velocity distribution.

This design method had several difficult aspects. One aspect was to specify a velocity distribution that actually corresponded to a physically-possible blade geometry. Many distributions that appeared optimum were found to be impossible physically. The

criteria that needed to be satisfied for a physical blade were: positive blade thickness everywhere, a completely enclosed (continuous) contour, and a higher average velocity in the channel between blades than the velocities upstream and downstream of the blade row[3].

Another consideration was to create a blade with the necessary turning. Increasing the area between the suction side and pressure side velocity distributions corresponded to an increase in blade loading and flow turning. Therefore, β_2 was very sensitive, changing with each modification of velocity. The target β_2 values (from the 1-D design phase) were each a challenging target to locate and maintain during velocity modifications.

A third consideration was to create an acceptable blade shape. The so-called "controlled-diffusion" blade shape was selected as the target shape. The name comes from the fact that the deceleration of the flow on the suction side is controlled. The diffusion should be controlled because a steep flow deceleration can cause separation. In the separated region, the flow no longer follows the blade surface, so the blade does not turn the flow, and therefore no pressure rise can occur. If there is no reattachment following the separation, the flow will remain separated for the remaining length of the blade. Therefore, separation near the leading edge is worse than separation near the trailing edge. Besides avoiding steep decelerations, the controlled-diffusion blade removes unnecessary positive accelerations on the suction side, because extra acceleration has to be compensated for with extra deceleration. Although the suction side was the most critical side for controlling diffusion, attention was also paid to the pressure side deceleration.

The final consideration of the inverse design method is that the blade created should have an appropriate thickness and overall shape. Higher designed velocities on the blade surfaces translate to more flow blockage in the channel, resulting in thicker blades. A blade that is too thin would break or deform on impact with any of a number of small particles and airborne objects that are present in the air near the streets and roads where the fan would see usage. Figure 1 shows a tip-section design which was too thin, along with its velocity distribution. Besides the fact that it is too thin, the very high peak in non-dimensional velocity at the leading edge ($W/W_1 \sim 15.0$) is very undesirable. On the other hand, a blade that is too thick adds unnecessary weight and material cost to the fan design. The stresses due to the centrifugal force on blades with varying contour thickness across the span would also be higher than constant thickness blades, possibly lowering the lifespan of the blades. An example of a thick blade and its velocity distribution is seen in Figure 2. Considering all aspects of the inverse design method and understanding their inter-relatedness only came with practice.

T/C=4.676 EL=77.9

Figure 1a

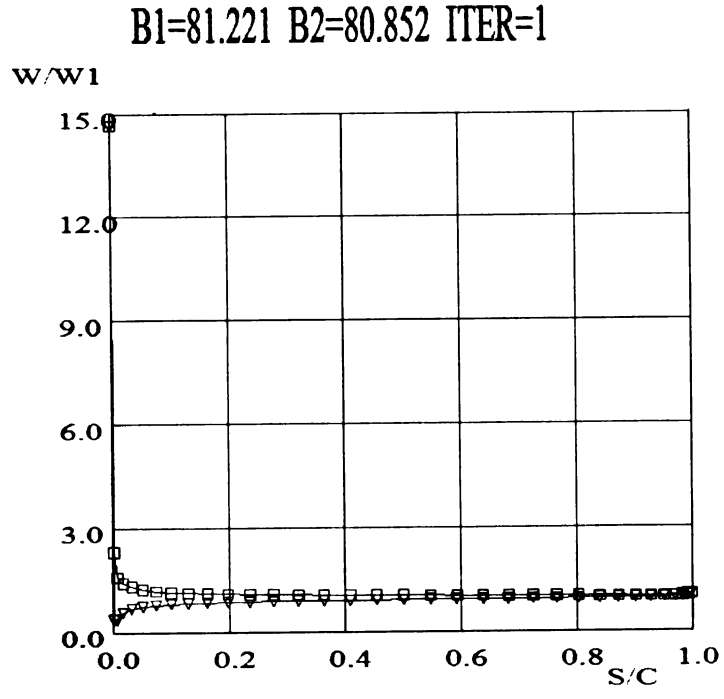

Figure 1b

Figure 2a

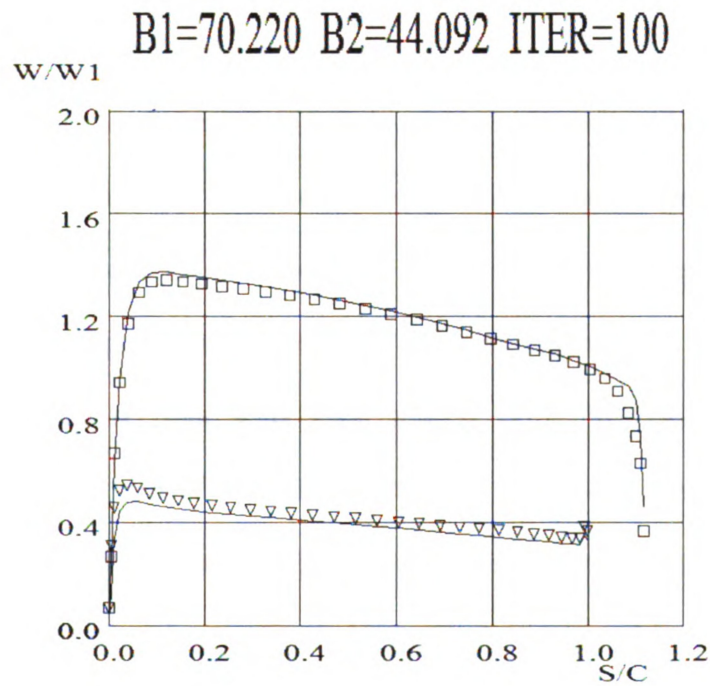

Figure 2b

Due to the fact that the 2-D design process used an inviscid code, each blade section was analyzed using the 2-D Navier-Stokes(N.S.) flow solver software TRAF2D. Preparing for and performing the analyses required several steps including: data transfer, inviscid grid generation, viscous grid generation, flow calculations, and post-processing.

Step one for analyzing the flow of each blade section was transferring the blade data from the form that was produced by INVC to a form suitable for the N.S. flow solver. Again, a small program was written to re-order the blade coordinates from the INVC.OUT file and print them into an airfoil.dat file. Bearing in mind that the output from INVC included dimensionless coordinates of a blade section with (x = 0, y = 0) the location of the leading edge, some modifications needed to be made to the coordinates. The program ruota_prof was used to scale the blade coordinates to the correct dimensions. Then a program called fit.exe was used to locate the center of gravity of the section. Using ruota_prof and the coordinates of the center of gravity, the blade was translated in space to have the point (0, 0) located at the center of gravity of the section. The reason for the translation is that (0, 0) is the stacking point for the 3-D geometry to be performed after the 2-D geometry; for rotors the center of gravity is the logical stacking point with respect to the stresses due to centrifugal force.

The modified sections were then plotted using TECPLOT so that a visual inspection of the blade contours could be performed (Figure 3). On both the middle and tip sections there was a small discontinuity at the leading edge slightly toward the pressure side. Since there was a relatively large concentration of points near the leading edge of both sections, the points where the discontinuities were located were adjusted to

make a continuous curve without significantly altering the blade shape. The result was a smoother surface at the microscopic level of the pressure side of each of the two blade contours.

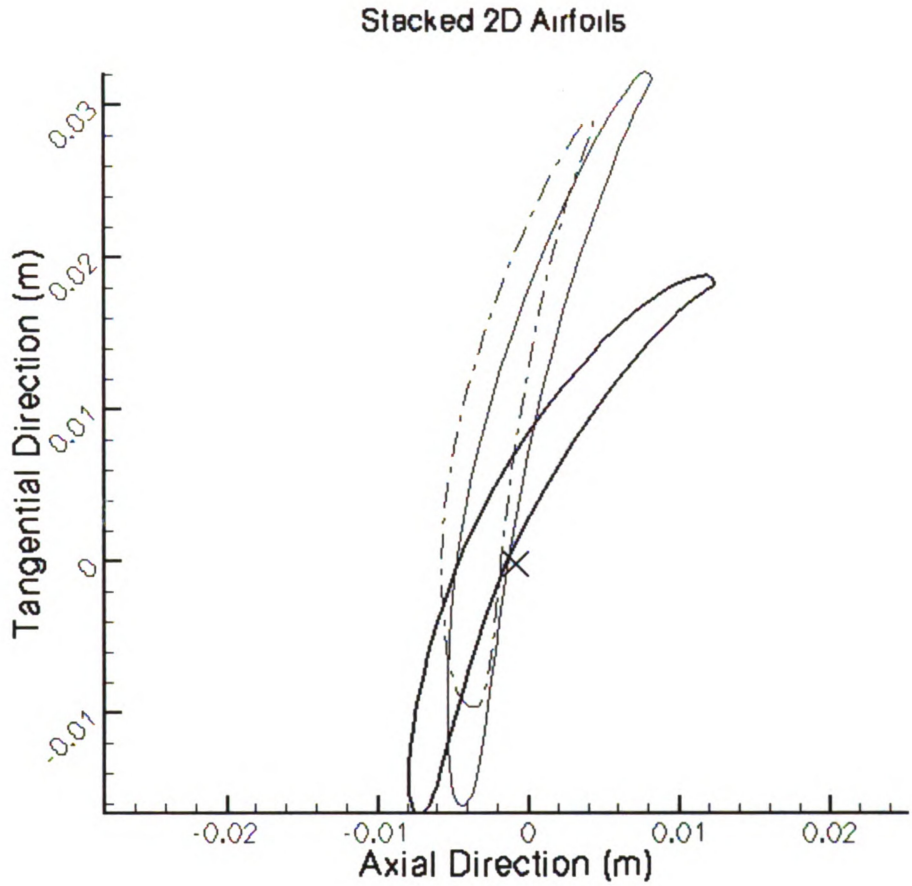

Figure 3

The next step was to create an inviscid mesh (grid) for the flow around each section using the program jerryh_tec. An H-mesh was chosen because it is more suited to the geometry of compressor blades than the C-mesh, which is typically used more for blades with rounded leading edges such as turbine blades. Keeping in mind that eventually the blade sections would be stacked together for the 3-D analysis, the node distribution was maintained constant from one section to the next. This was necessary because the grid stacking program interpolates between sections to form the intermediate

mesh and therefore requires that the same number of nodes be present on a given surface at each radial position. The nodal distribution was specified for 6 surfaces: inlet lower (ninl in Figure 4), inlet upper (ninu), suction side (nss), pressure side (nps), wake lower (nw), and wake upper. In addition, the number of points across the blade channel was specified (ny). An example of the different parameters is shown for a turbine blade in Figure 4.

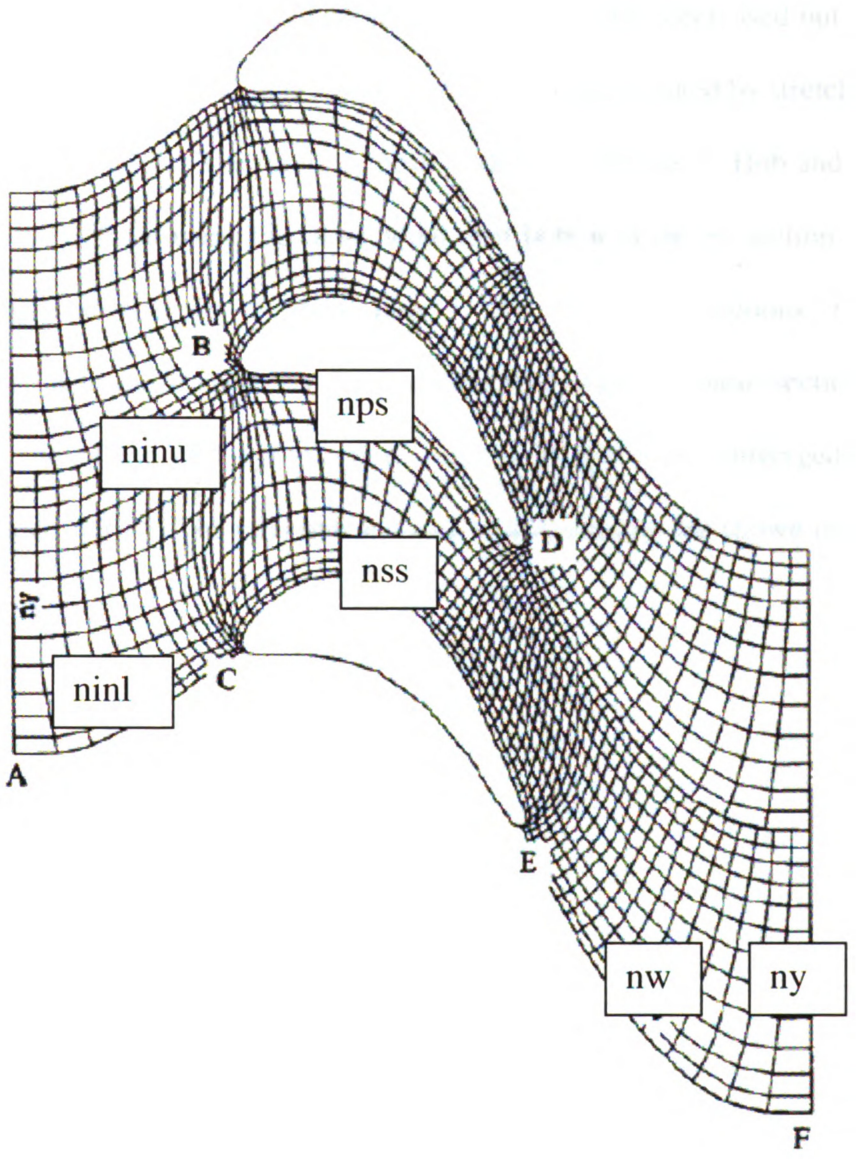

Figure 4

The initial mesh generation work was done on the tip section. Because of its extremely high stagger angle (78.5 degrees), it posed the biggest challenge for generating an optimum mesh. The first grid with default values was severely non-orthogonal and full of negative volumes at the leading edge. However, orthogonality was drastically improved by changing the nodal distribution on the surfaces mentioned previously. The number of nodes was increased on the inlet upper surface and wake lower surface and decreased everywhere else. The number of negative volumes thus decreased but did not disappear completely. The remaining negative volumes were eliminated by stretching the cells around the leading edge. The final tip mesh is shown in Figure 5. Hub and middle section meshes were defined using the same nodal distribution as the tip section (for the 3-D grid stacking and analysis to come later). For these two sections, the grid orthogonality was made much easier by the lower stagger angles of these sections than the tip. By the end of the grid optimization, each mesh was well converged with a residual on the order of 10^{-6}. The final hub and mid section meshes are shown in Figures 6 and 7, respectively.

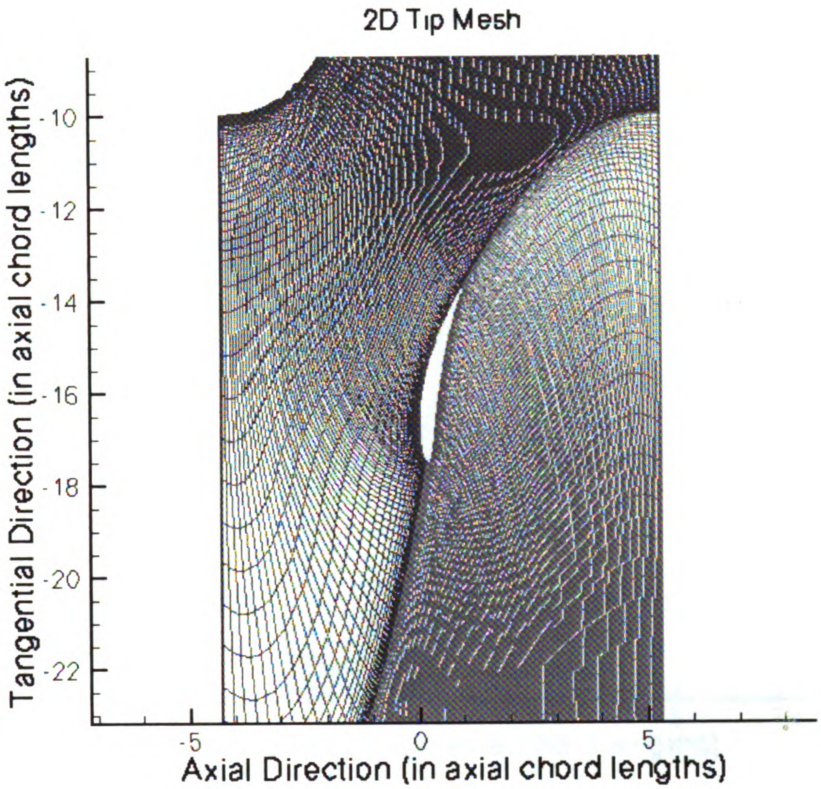

Figure 5

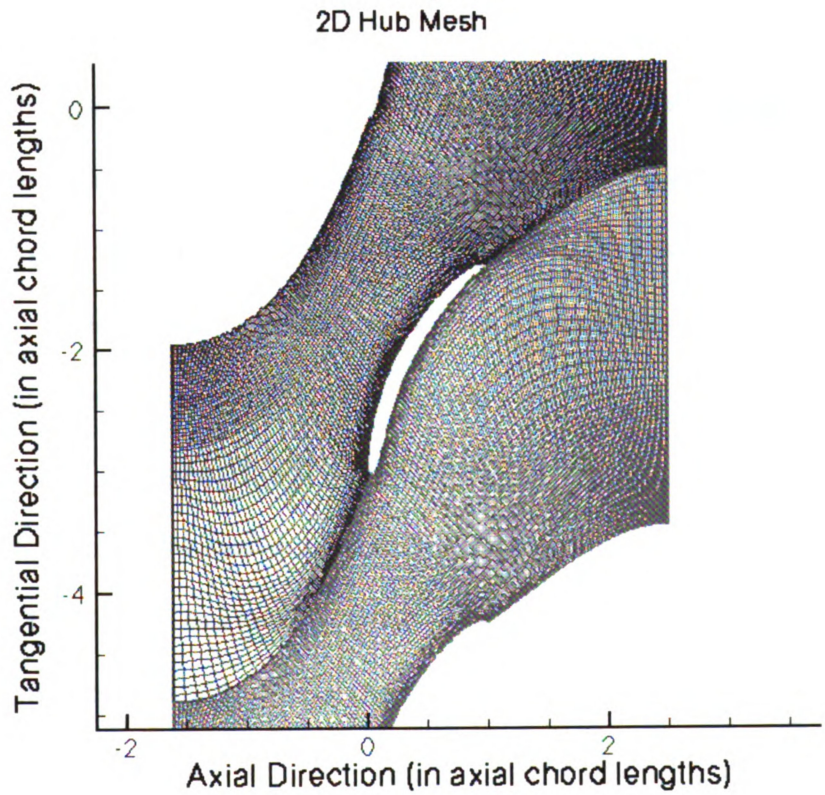

Figure 6

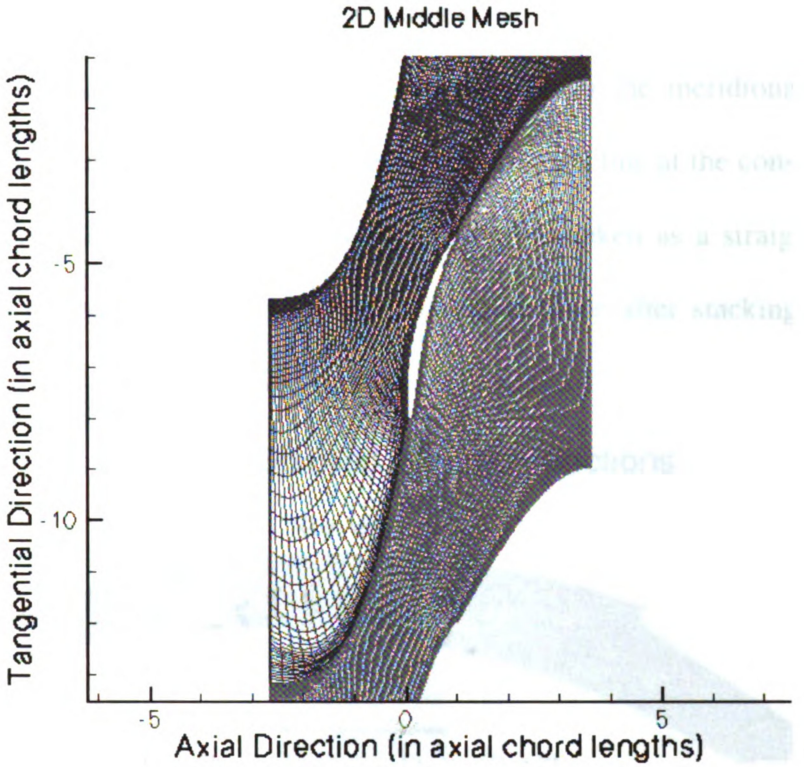

Figure 7

The viscous mesh was created based on the inviscid mesh using tomh_tec. Starting with the viscous grid, a new number of points across the channel was specified as well as a stretching factor to compress the grid near the blade surfaces and periodic boundaries. Again, the number of points in the tangential direction across the channel was required to be the same from section to section for mesh stacking. The meshes were then each ready for an individual 2D flow analysis.

4.2.3 3-Dimensional Stacking of 2-Dimensional Grids

The stacking process had already been started thanks to the earlier considerations of the stacking point (0, 0) and the continuous number and location of nodes/cells relating each blade section to the others. Still, a new minor modification was needed. Ideally, the inlet and outlet planes of the final, stacked blade would be straight, radial planes, so each inlet and wake axial length was calculated and adjusted to meet that criterion. After the

mesh files were ready to be stacked, the number of cells in the radial direction, the number of blades Z, and the contour of the end-walls in the meridional plane were specified. The hub end-wall contour was taken as a straight line at the constant radius of the hub section, while the shroud end-wall contour was taken as a straight line at the constant radius of the shroud section. An individual blade after stacking is shown in Figure 8, and the full fan is shown in Figure 9.

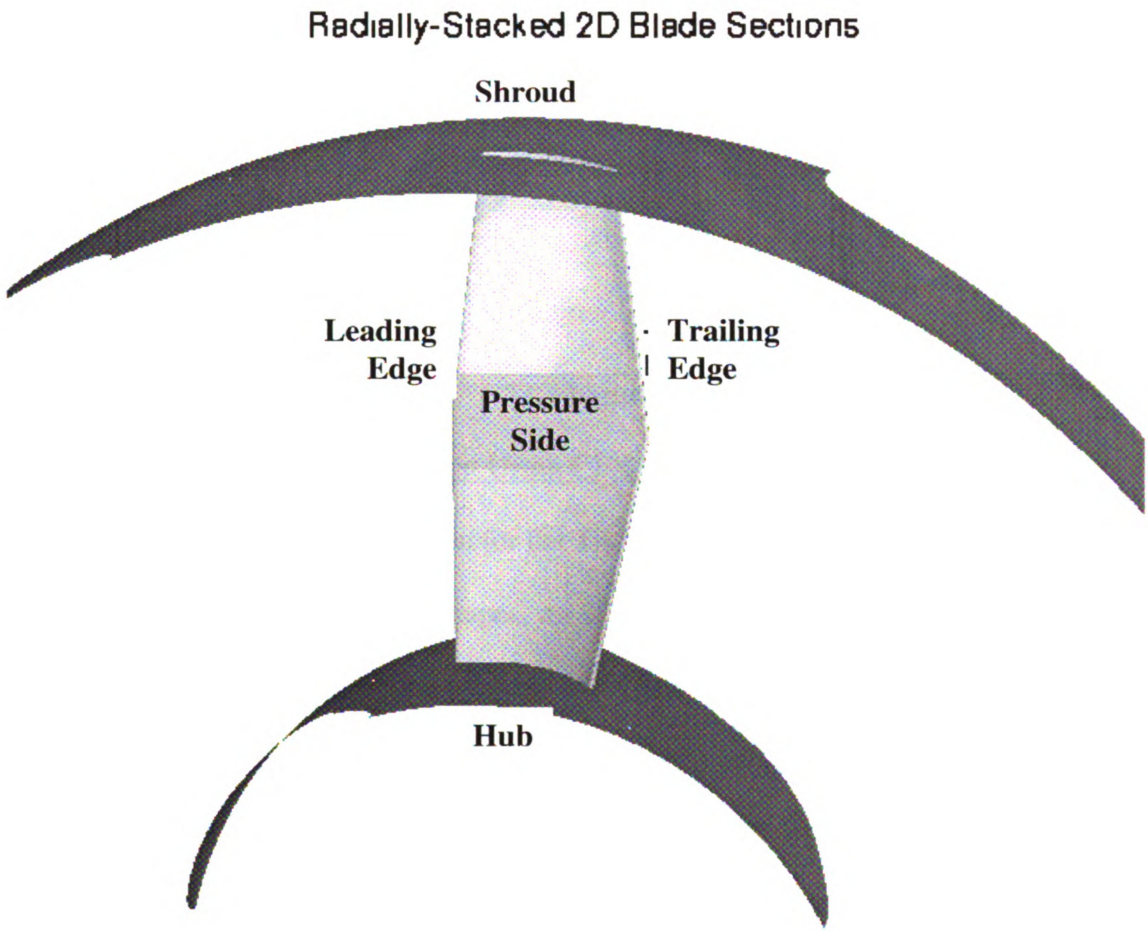

Figure 8

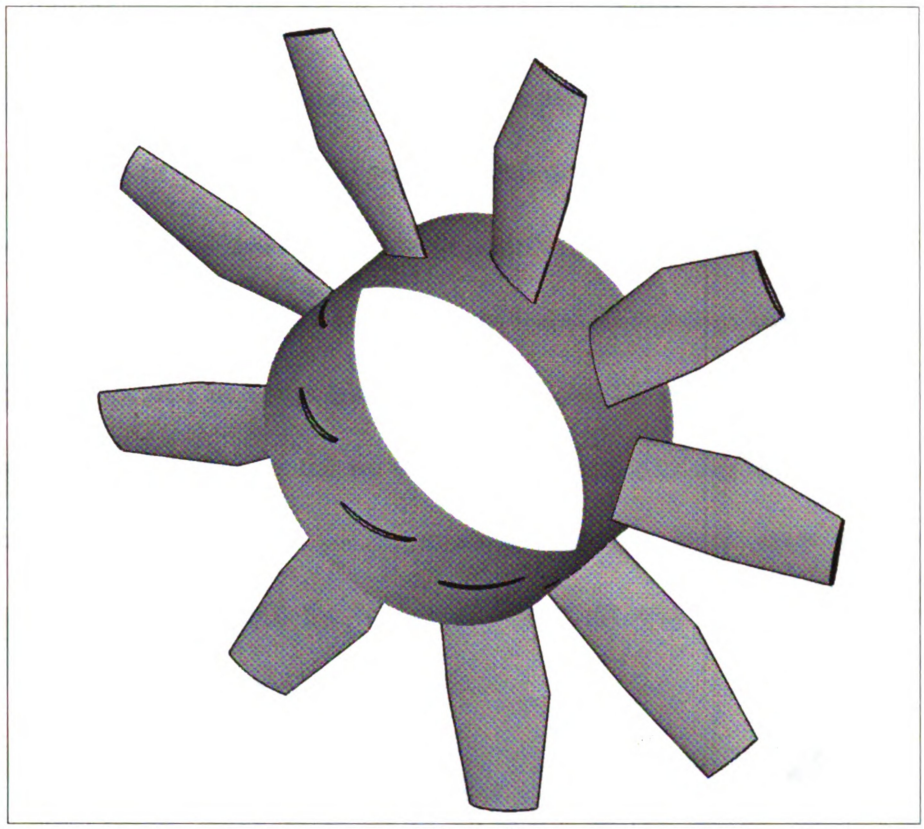

Figure 9

4.2.4 3-Dimensional Grid Generation Using CFX Turbogrid

Similar to the grid generation for the TRAF software, the CFX grids required inlet files specifying the 2-D contour shapes, as well as the hub and shroud contours in the meridional plane. The difference was that the TRAF input contour coordinates were all taken on a constant-radius plane and thus required only two coordinates: an axial coordinate and a circumferential coordinate. Instead, CFX Turbogrid required the axial coordinate, a "horizontal" coordinate, and a "vertical" coordinate. The transformations shown in equations 14-17 were used. Each section's center of gravity point ($x_{TRAF} = 0$, $y_{TRAF} = 0$) was defined as the point ($f = 0$, $z_{CFX} = r$, $y_{CFX} = 0$) in the CFX system. Again, a program was written to store the new coordinates into a profile.curve file to be read by the CFX Turbogrid program.

Unlike the TRAF mesh sections, the CFX mesh sections were interpolated from two meshes: the tip section mesh and the hub section mesh. The combination of H and J type meshes proved to fit well to the tip section mesh, so it was used for the entire blade. To remove negative volumes and improve orthogonality, control points were created and moved accordingly. Figures 10 and 11 show the hub and tip mesh sections, respectively. The small spheres located at some nodes were the control points. Areas that were especially non-orthogonal, such as the tip section wake and inlet meshes, required many control points and modifications. Intermediate meshes were then interpolated automatically, and each resulting mesh section (10 total) was modified with control points where negative volumes occurred.

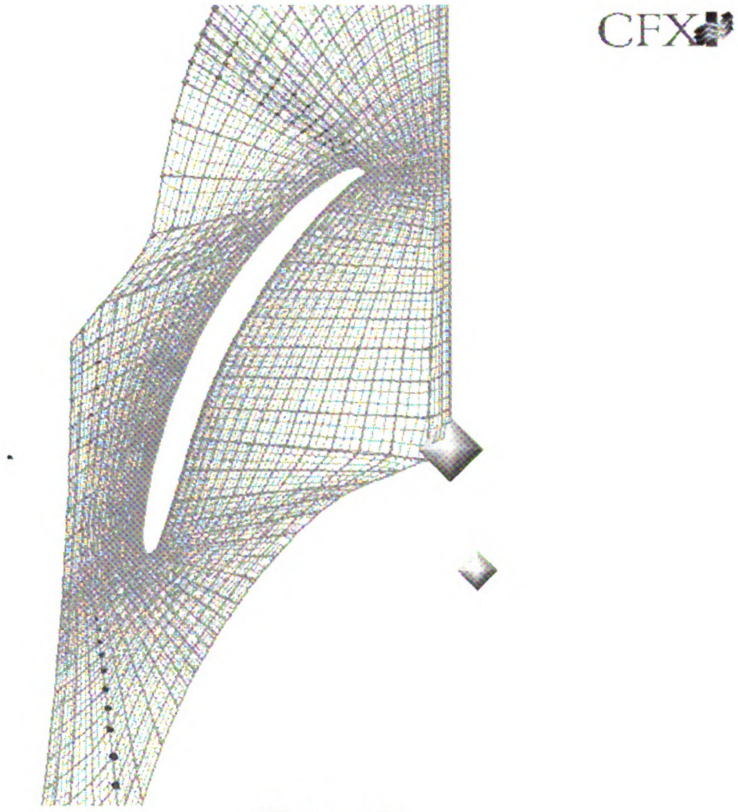

Figure 10

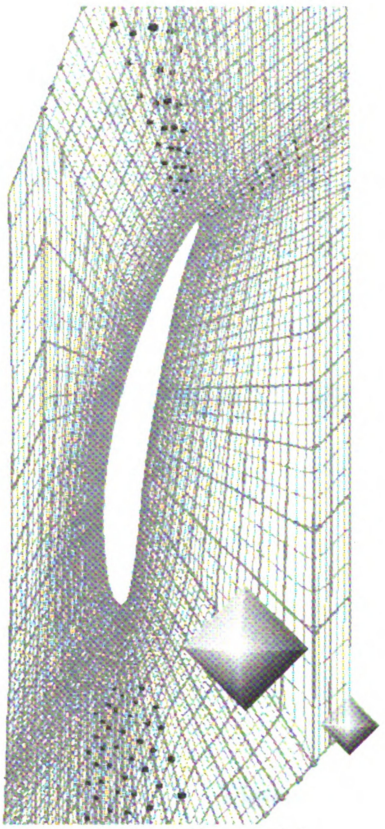

Figure 11

4.3 Results

4.3.1 2-Dimensional Inverse Design

The hub section was the most critical and time-consuming section to design, because it would eventually serve as the basis for the other sections to be designed from. Very small changes in the velocity profile were often enough to change a blade from a close-to-optimum design to an unusable one. The target blade shape and performance were eventually met with the design shown in Figure 12.

T/C=1.431 EL=60.8

Figure 12a

B1=70.220 B2=48.725 ITER=100

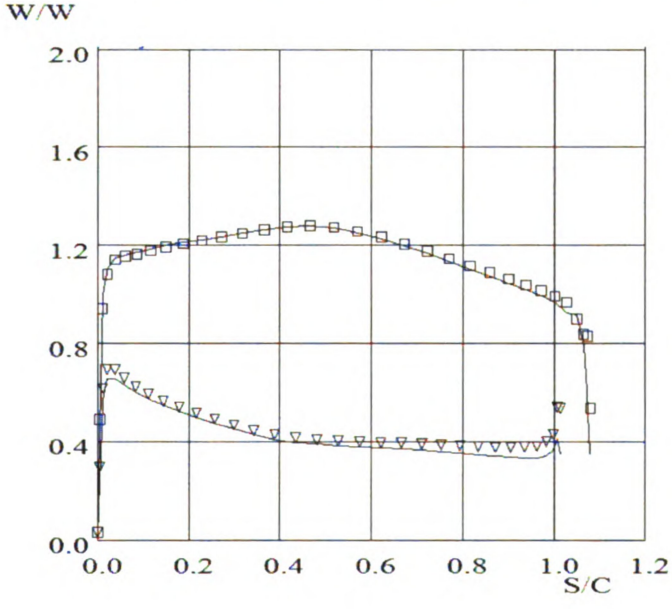

Figure 12b

After the target design was achieved for the hub section, the middle section was designed based on the hub section by modifying the camber and stagger. A program was created to take coordinates of the hub section at zero stagger and scale the y-component (normal to chord line) of each point by a certain factor of its original value. The program then automatically wrote the new coordinates to a text file that could be read by INVC. The re-staggering was implemented directly in the INVC file. The scale factor used for the middle section was 70% of the hub camber while the factor for the tip section was 55%. The scaling served to not only change the camber angle, but also the thickness of the sections, providing a favorable evolution of blade thickness from hub to tip. The middle and tip sections were then analyzed using INVC, and a velocity peak was found at the leading edge of the tip section (Figure 13). A few modifications with INVC-MOD removed the peak and established the controlled diffusion velocity profile and final tip contour shape, seen in Figure 14. The final middle (reference section) contour is shown in Figure 15.

T/C=3.333 EL=78.5

Figure 13a

B1=81.221 B2=80.049 ITER=1

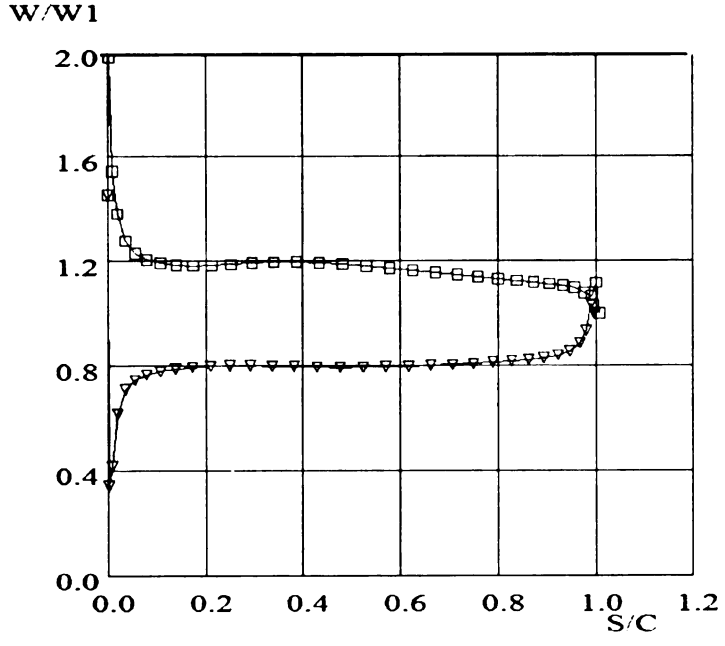

Figure 13b

T/C=3.333 EL=78.5

Figure 14a

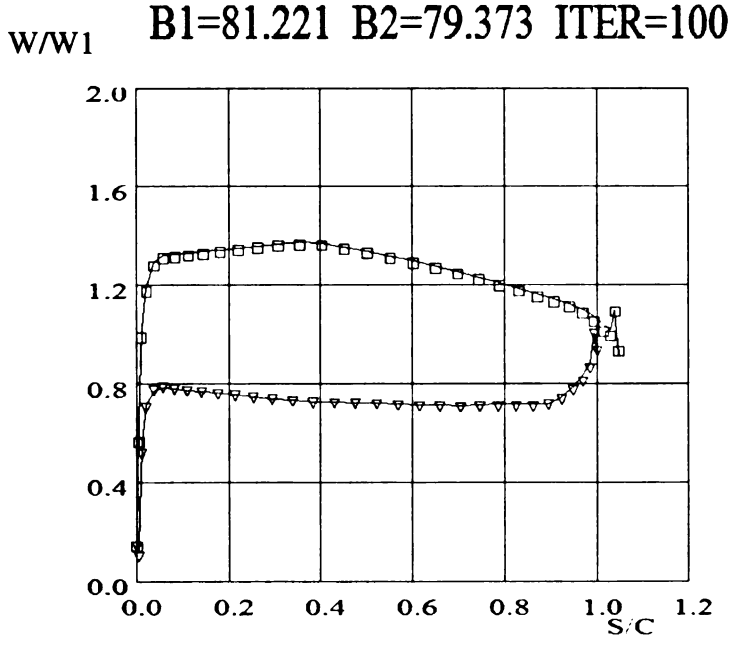

Figure 14b

Figure 15a

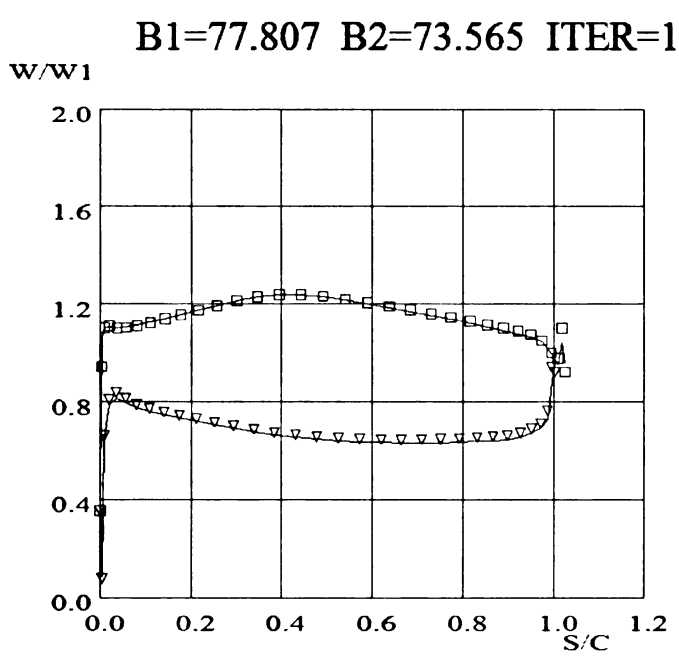

Figure 15b

4.3.2 2-Dimensional Analysis: TRAF2D

The purpose of creating a TRAF2D solution for each section was to see if the blade sections performed the same as the inviscid design predicted when viscosity was added. The comparisons of blade surface velocity distributions can be seen in Figures 16-18. The hub surface velocities compare well with the designed velocities, as do the middle section's velocities. However, near the trailing edge of the middle section suction side there is a velocity plateau, signifying that the flow has separated from the surface and is providing no pressure rise in that region. The tip section's profile does not match the inviscid design very well at the leading edge, which is an issue of incidence. Because the area between the velocity curves is smaller for the viscous solution than the inviscid design, the work being done by the blade on the flow is less than specified.

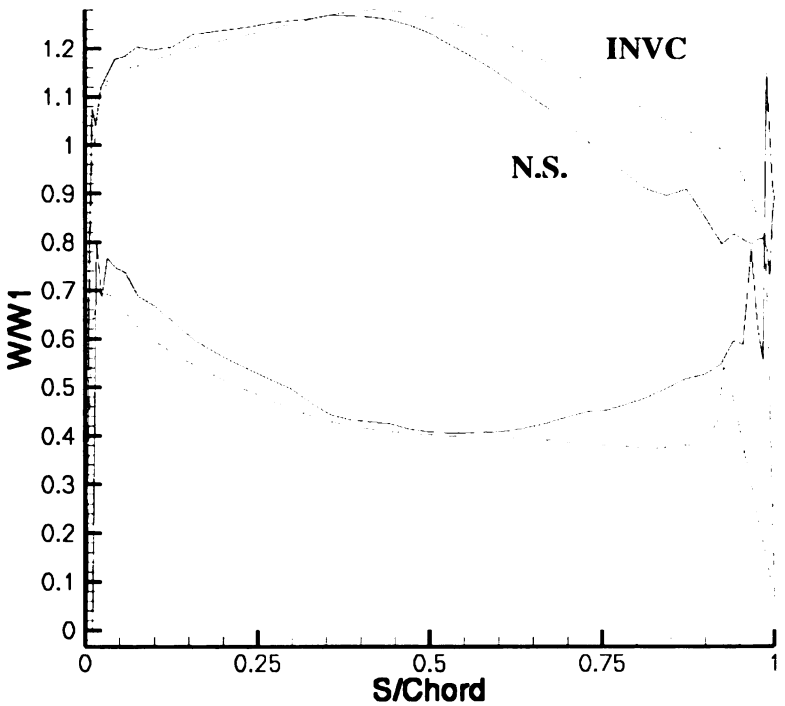

Figure 16

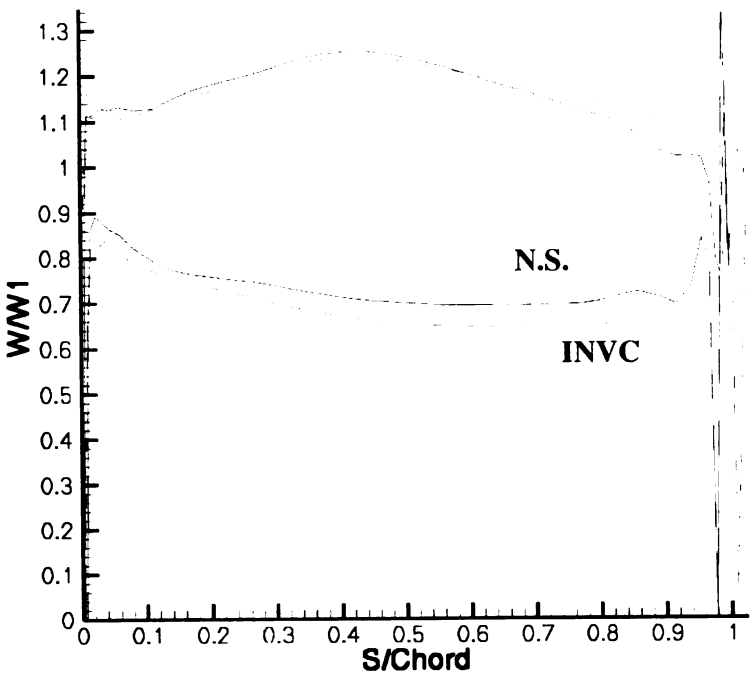

Figure 17

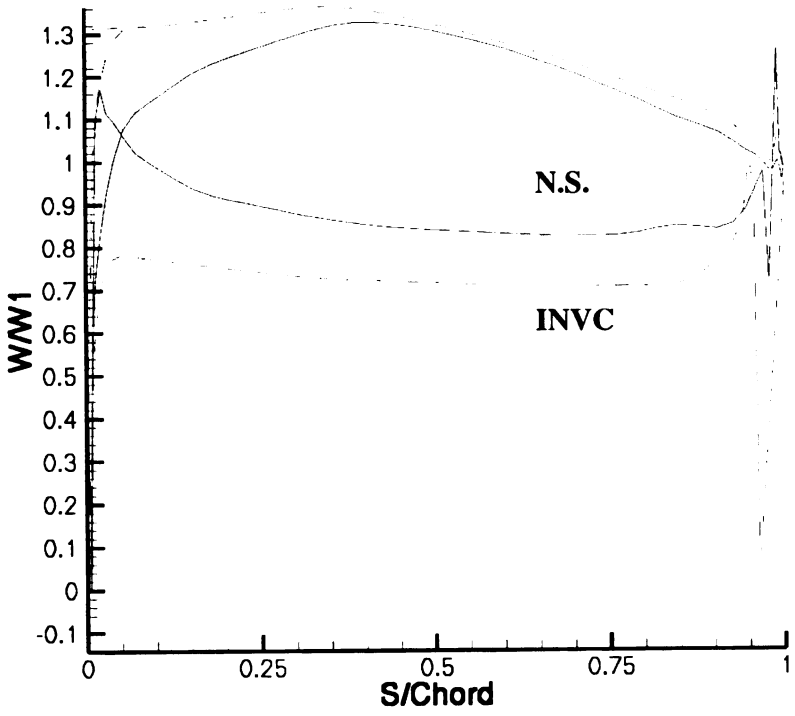

Figure 18

The Mach number plots provide a good idea of what the flow is doing in the inlet, channel, and wake. In each plot there is a good indication of where the leading edge stagnation point is, characterized by a zone of low velocity. On the suction side, the acceleration followed by deceleration can also be clearly seen.

4.3.3 3-Dimensional Analysis: TRAF3D and CFX

The 3-D analysis was done using the TRAF3D and CFX software packages. The TRAF3D convergence history is shown in Figure 19, and the CFX convergence is shown in Figure 20. A stable solution was reached by 800 iterations for both computations. The seemingly discontinuous drop in logarithms of RMS at 200 iterations results from the solver switching from the course grid to the fine grid. The required mass flow rate of 0.84 kg/s was achieved with both solvers but at different pressure ratios. The TRAF3D solution yielded a static pressure rise of 78.547 Pa while the CFX solution gave 118 Pa. The values were averaged in the circumferential direction at the inlet plane, taken at 25% of the hub section axial chord upstream of the leading edge, and at the outlet plane, taken at 25% of the hub section axial chord length downstream of the trailing edge. The TRAF3D values are presented in Appendix 5a and the CFX values are presented in Appendix 5b.

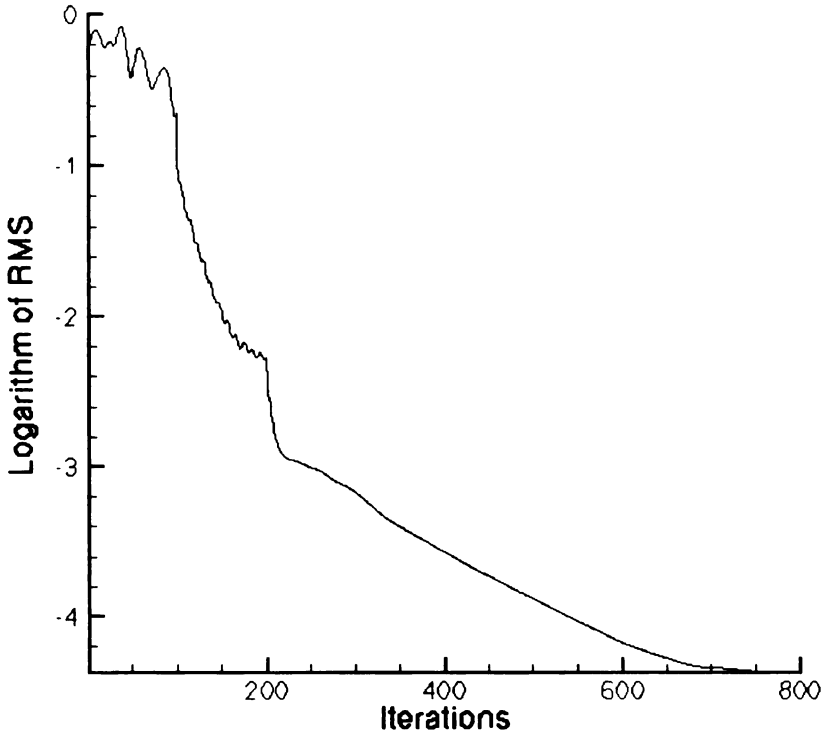

Figure 19

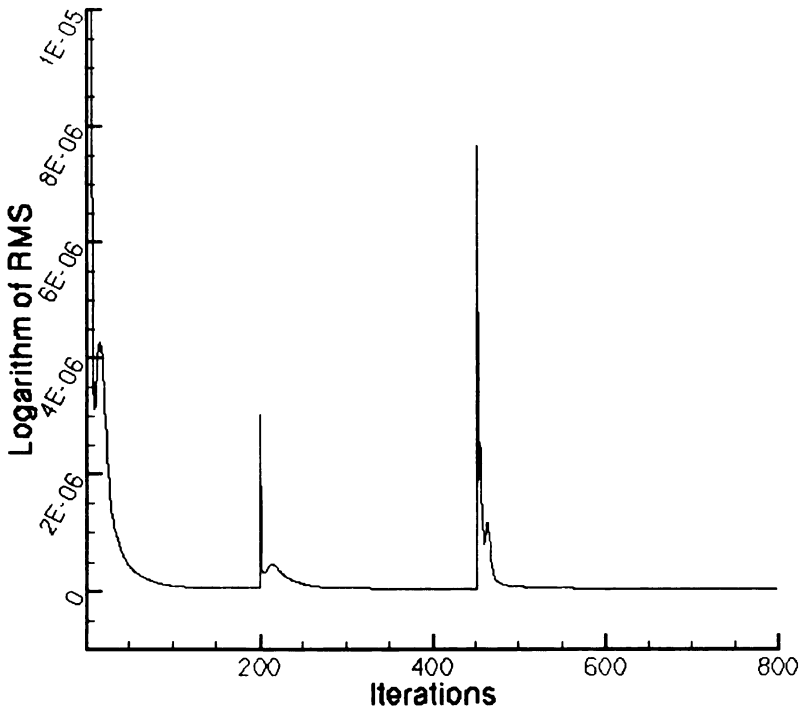

Figure 20

The efficiency was higher in the CFX result than in the TRAF3D result, as shown in Figure 21. In this figure and the following figures, the circumferentially mass-averaged values are plotted across the span of the blade. The definition of efficiency shown in equation 13 was employed. In the 1-D design, an efficiency of 70% was assumed. While a higher average efficiency was observed for the CFX solution (77%), a lower average efficiency was observed for the TRAF3D solution (49%). The main reason for the discrepancy is the fact that the static pressure rise was not as large for the TRAF3D solution as the CFX solution (Figure 22) due to hub and shroud end-walls rotating farther upstream for the TRAF3D solution. In the TRAF3D case, the energy from the rotating inlet walls was transferred into a temperature rise (Figures 23 and 24) and pre-swirl instead of a pressure rise. There was an averaged total temperature increase of 0.409 K, which seems insignificant but is enough in such a low pressure-rise machine to reflect a reduction in efficiency. The total pressure rise can be seen in Figure 25.

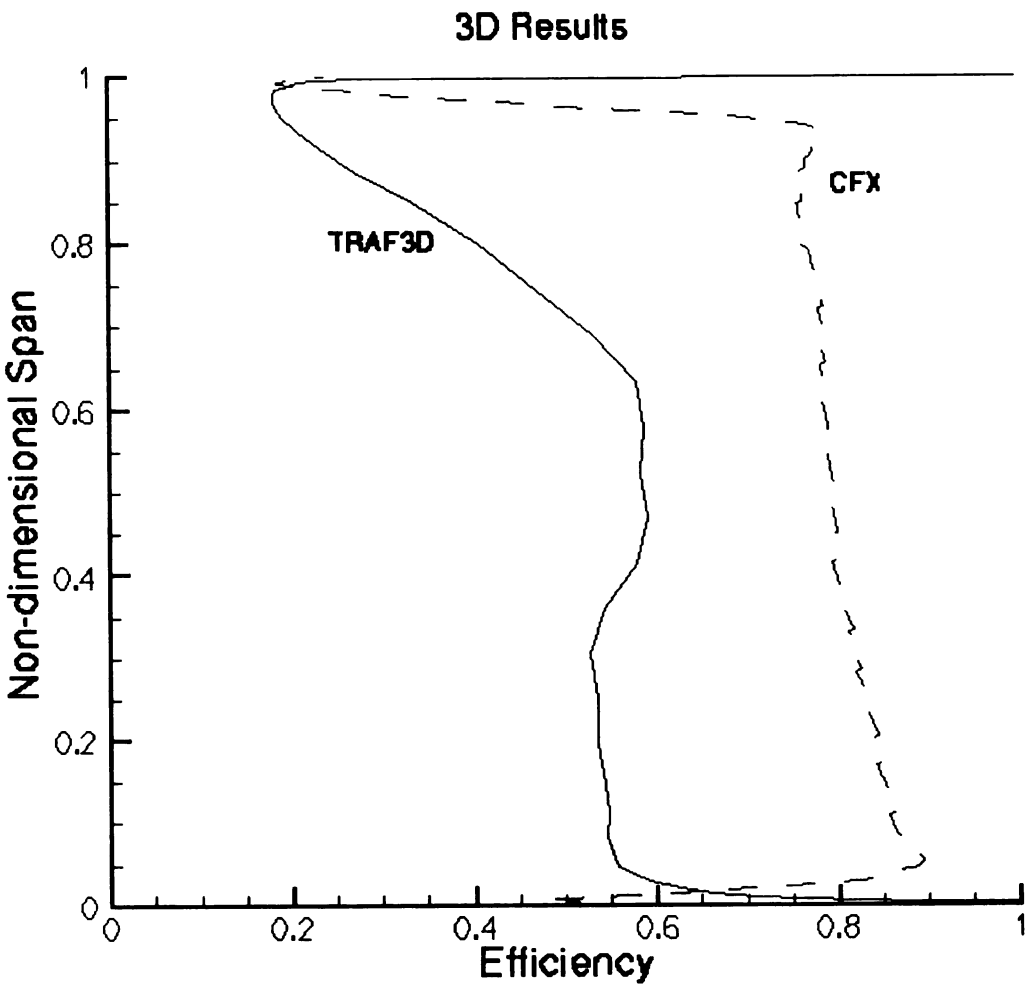
3D Results
CFX
TRAF3D
Non-dimensional Span
Efficiency
0
0.2
0.4
0.6
0.8
1

Figure 21

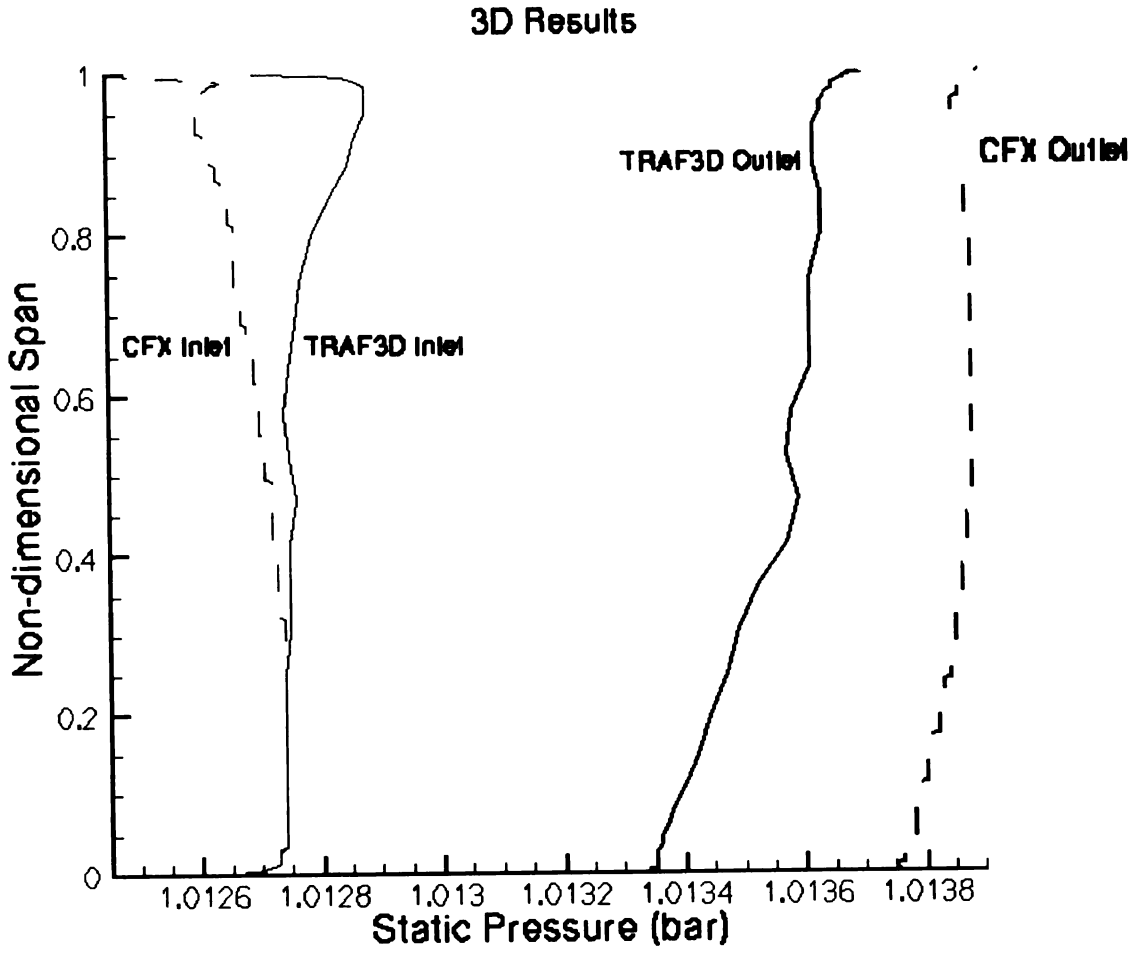
3D Results
Non-dimensional Span
Static Pressure (bar)
CFX Inlet
TRAF3D Inlet
TRAF3D Outlet
CFX Outlet
0
0.2
0.4
0.6
0.8
1
1.0126
1.0128
1.013
1.0132
1.0134
1.0136
1.0138

Figure 22

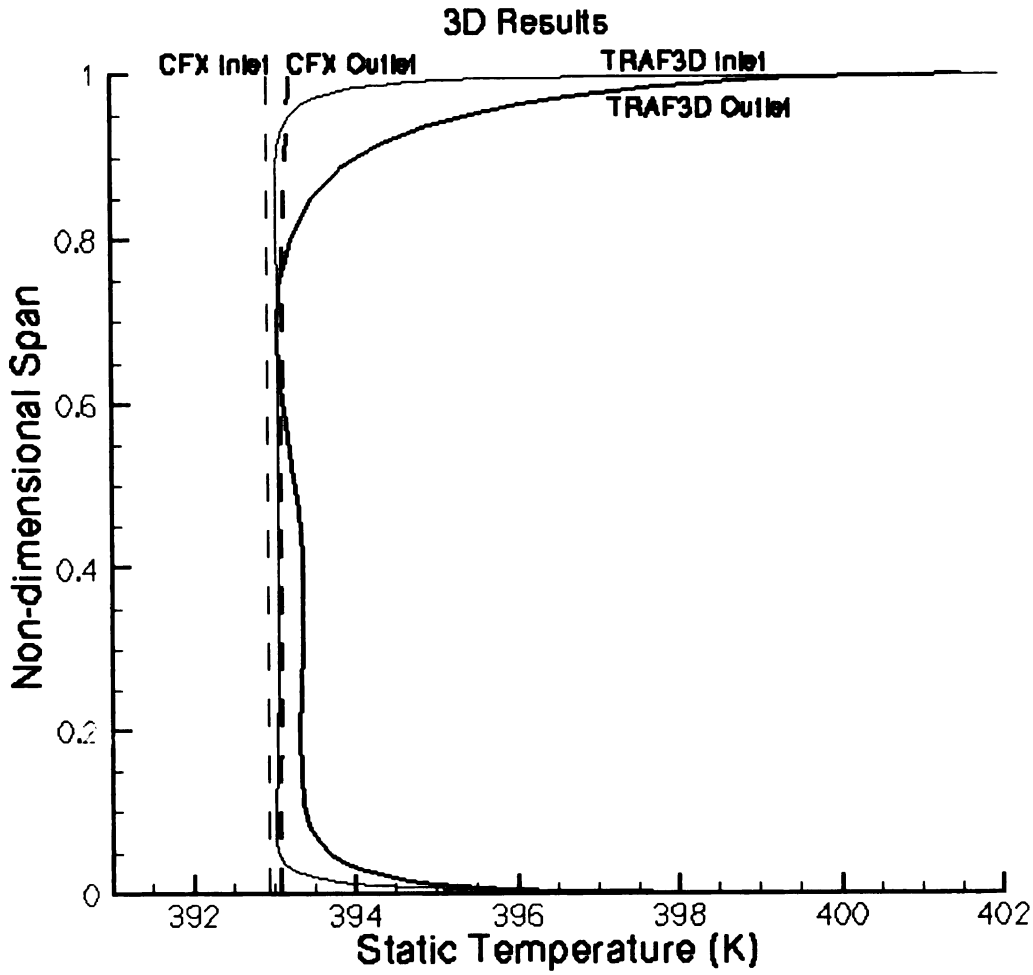
3D Results
CFX Inlet
CFX Outlet
TRAF3D Inlet
TRAF3D Outlet
Non-dimensional Span
Static Temperature (K)
0
0.2
0.4
0.6
0.8
1
392
394
396
398
400
402

Figure 23

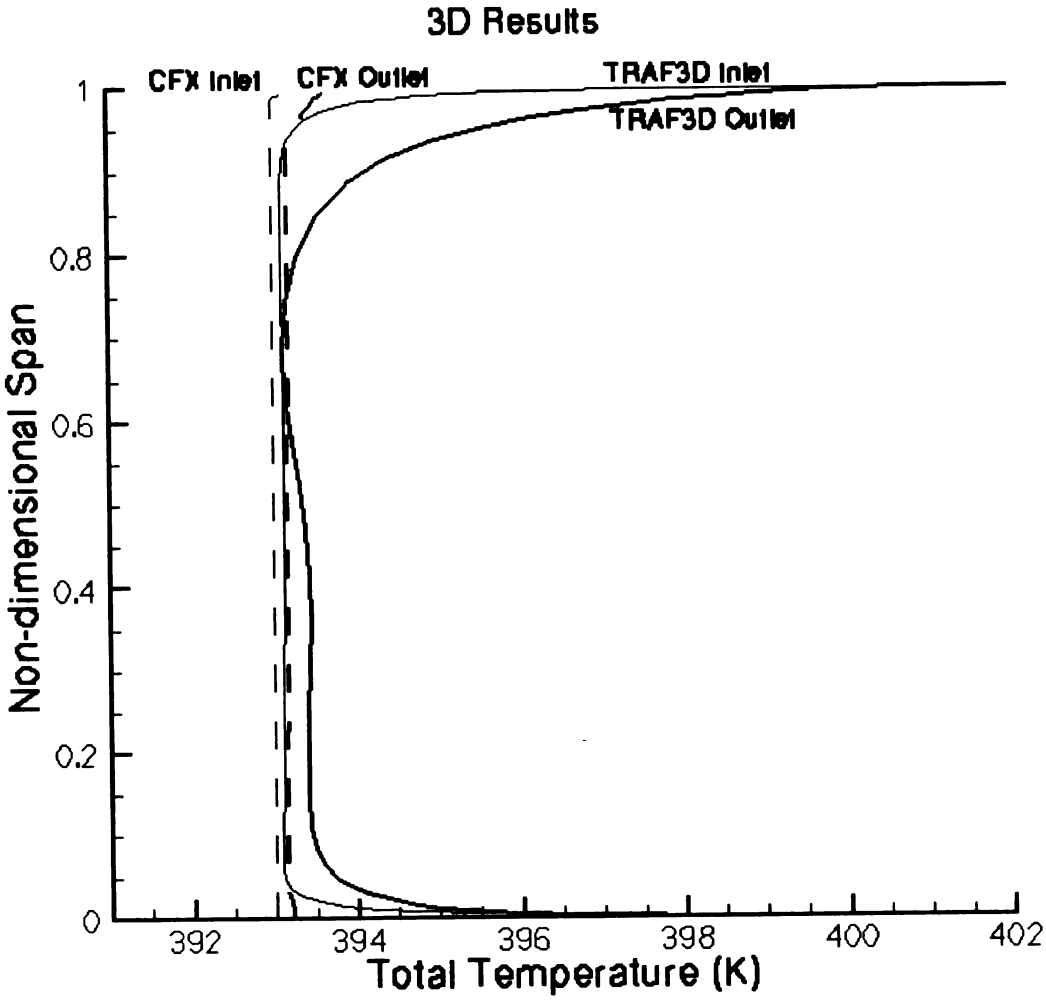
3D Results
CFX Inlet
CFX Outlet
TRAF3D Inlet
TRAF3D Outlet
Non-dimensional Span
Total Temperature (K)
0
0.2
0.4
0.6
0.8
1
392
394
396
398
400
402

Figure 24

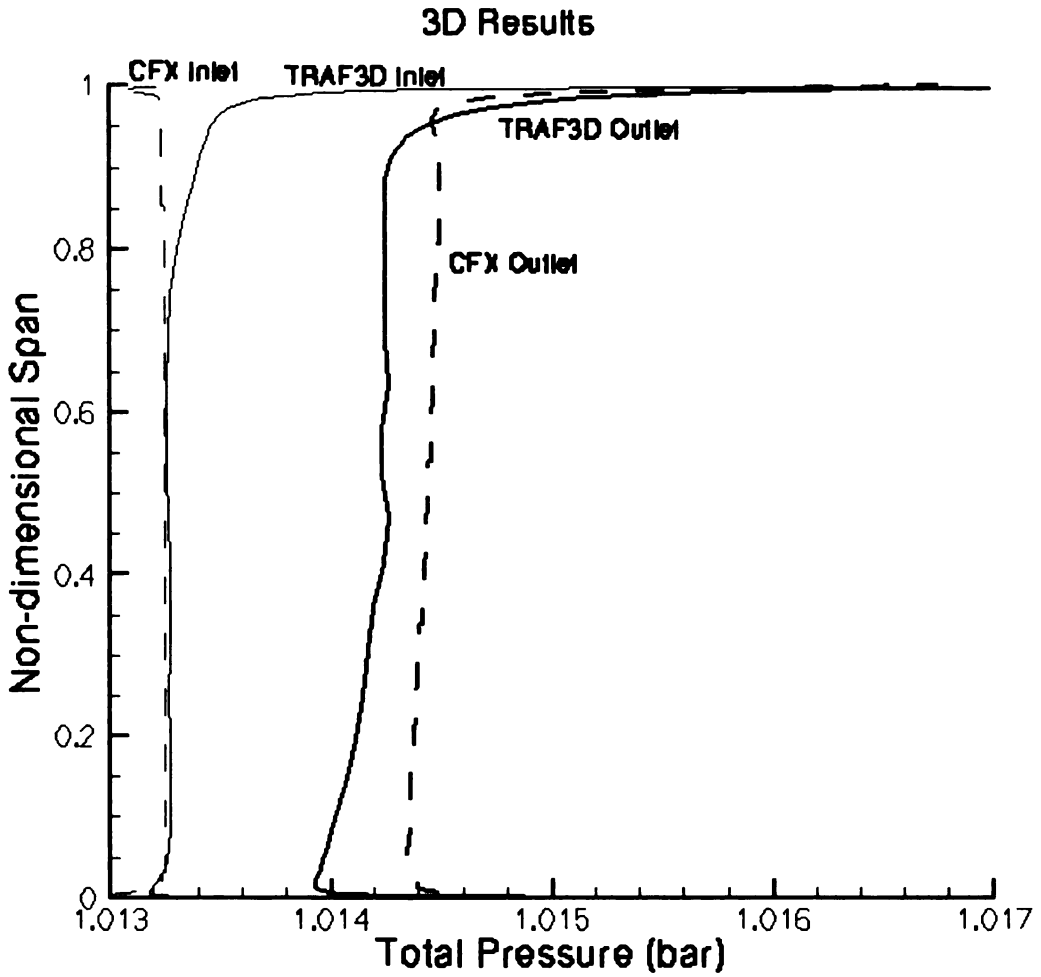

Figure 25

As well as producing a relatively low pressure rise, the fan operates at a very low mach number. The absolute and relative mach numbers are plotted in Figures 26 and 27, respectively. There is a good agreement between the relative mach numbers predicted by CFX and TRAF3D in the channel, but near the walls the effects of the rotating inlet are evident for the TRAF3D case.

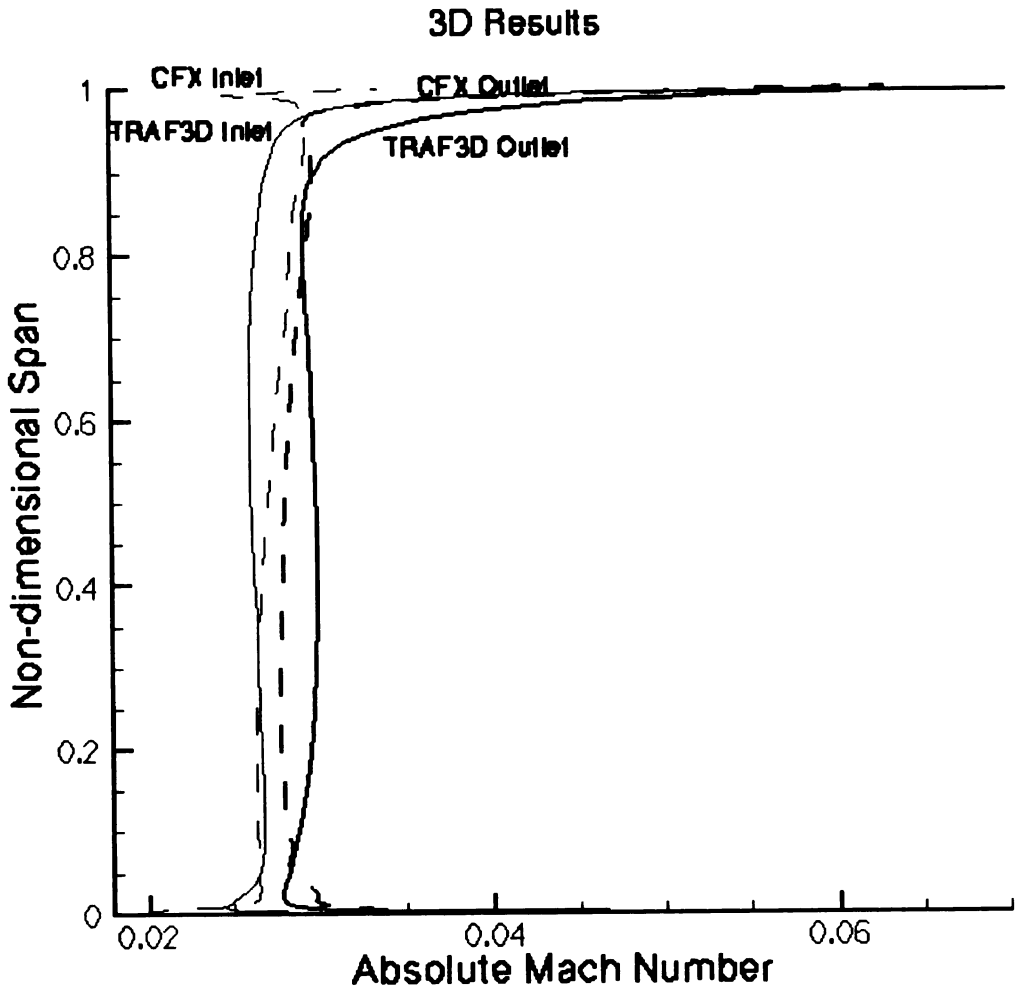
3D Results
CFX Inlet
CFX Outlet
TRAF3D Inlet
TRAF3D Outlet
Non-dimensional Span
Absolute Mach Number
1
0.8
0.6
0.4
0.2
0
0.02
0.04
0.06

Figure 26

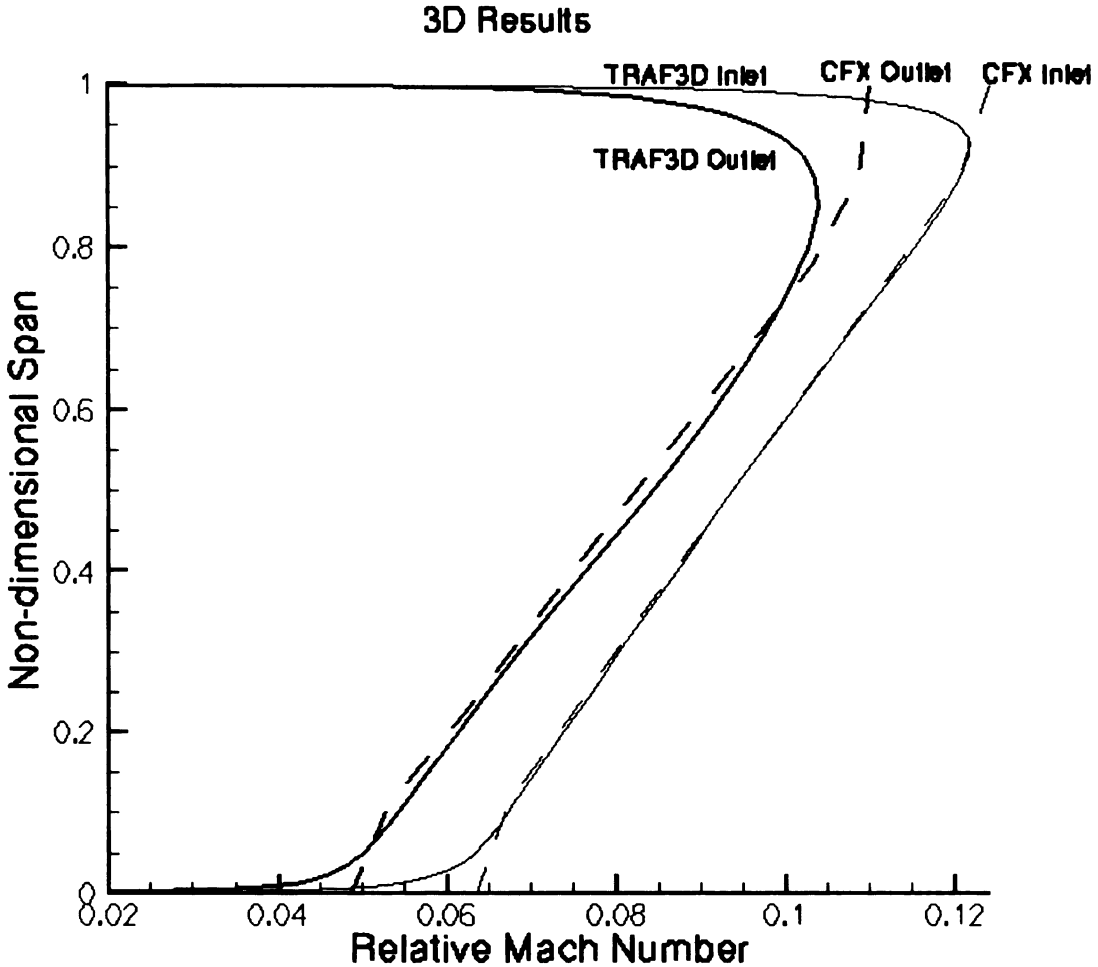

Figure 27

The evolution of absolute flow angles across the span of the blade are shown in Figure 28. The absolute flow angle is zero at the inlet, matching the uniform inlet flow specified. The effect of the rotating tip shroud is apparent in both the inlet and outlet absolute angles from the TRAF3D solution. Also, near both the hub and shroud walls the axial velocity is zero (Figure 29), but the absolute tangential velocity (Figure 30) is the same as the rotating walls (no-slip condition). Therefore, the absolute angles approach a negative infinite angle asymptotically near the hub and tip. These absolute outlet angles are closer to zero (more axial flow) than the 1-D design, which is a result of lowering the required pressure rise to get the required mass flow rate. The relative outlet flow angle

(Figure 31) increases almost linearly across the center of the span as expected due to the increase of rotor tangential velocity (U) with increasing radius. A significant area of relative flow angles is from about 90% span to the tip. Here, the difference in flow angles becomes negligible and then increasingly negative with radius, indicating that the flow is not turning correctly in the tip region. Compared to the 1D design, the calculated inlet relative flow angles are lower while the outlet relative flow angles are higher. Therefore the difference in outlet and inlet angles is lower than the 1D design, signifying that the blade is unloaded. This is correct, since the imposed static pressure rise was lower for both flow solvers than the 215 Pa in the 1-D design. The inlet angle near the tip decreases with increasing radius because flow has gained a tangential component before entering the blade passage due to the rotating shroud end-wall. The relative outlet angle increases more steeply near the tip than at mid-span as the axial velocity decreases in the boundary layer.

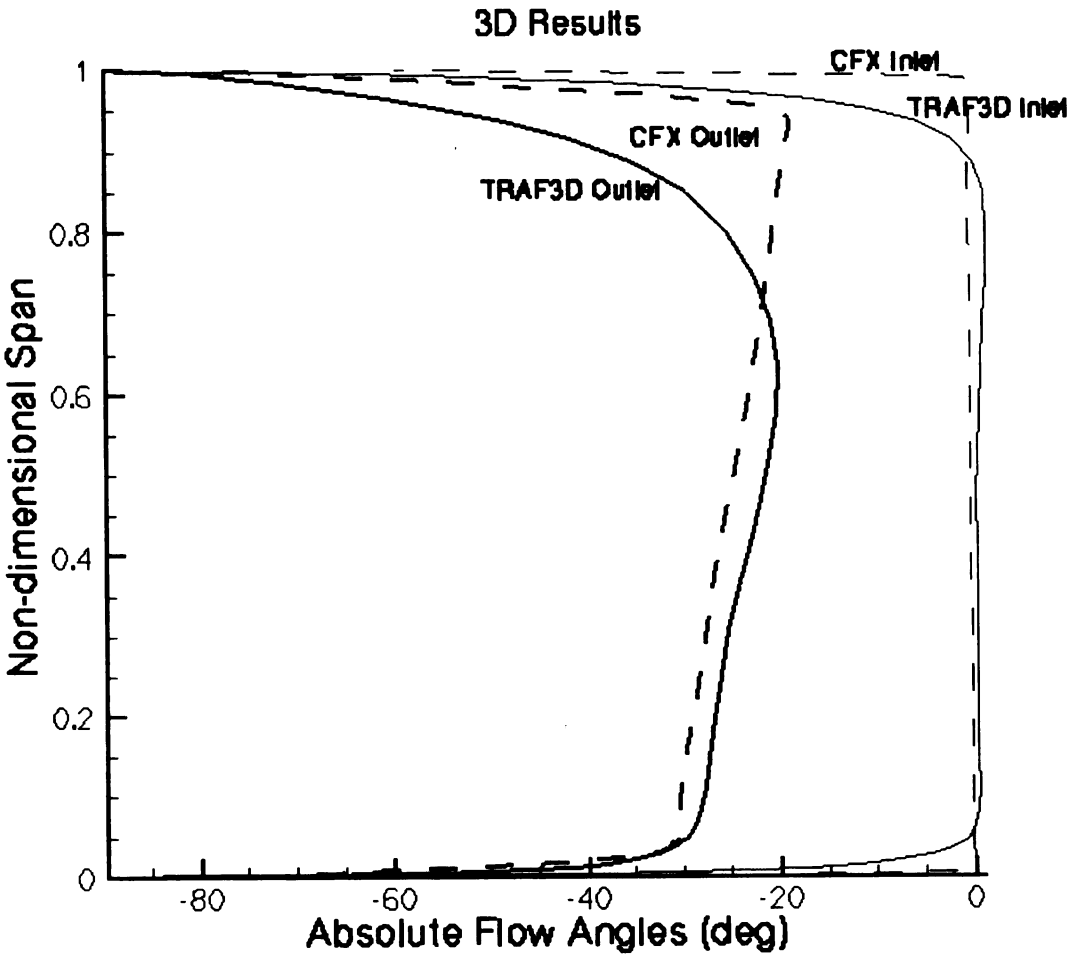
3D Results
CFX Inlet
TRAF3D Inlet
CFX Outlet
TRAF3D Outlet
Non-dimensional Span
1
0.8
0.6
0.4
0.2
0
-80
-60
-40
-20
0
Absolute Flow Angles (deg)

Figure 28

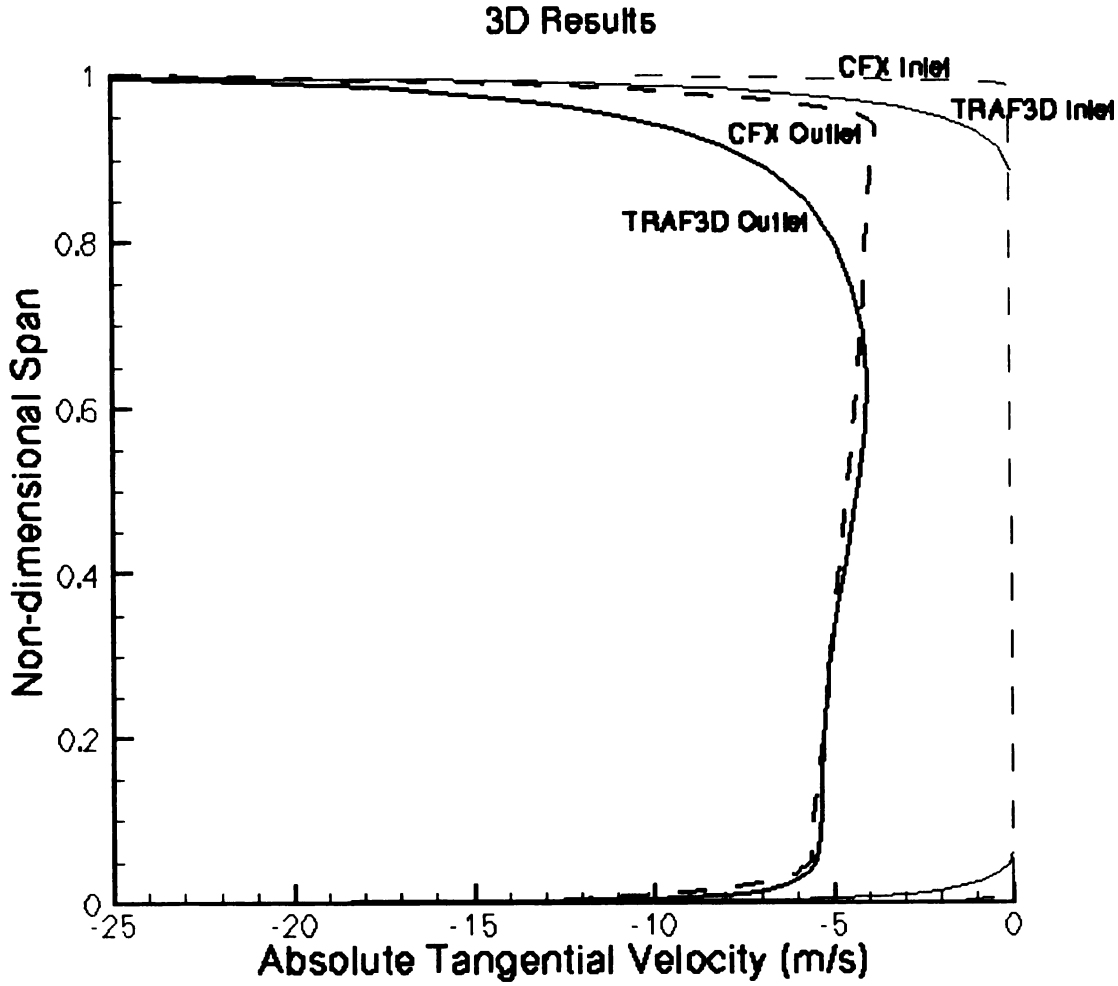
3D Results
CFX Inlet
TRAF3D Inlet
CFX Outlet
TRAF3D Outlet
Non-dimensional Span
Absolute Tangential Velocity (m/s)
1
0.8
0.6
0.4
0.2
0
-25
-20
-15
-10
-5
0

Figure 29

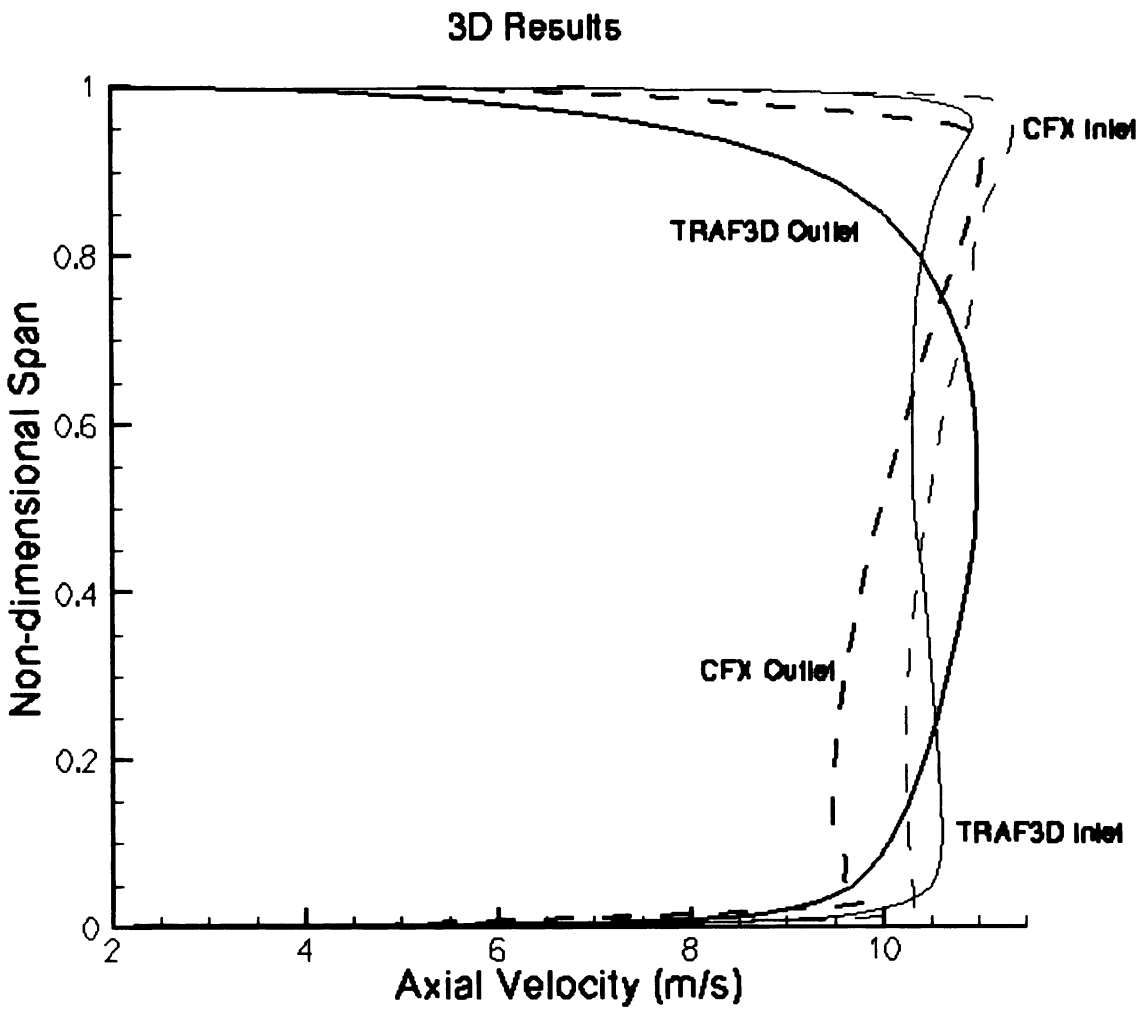
3D Results
CFX Inlet
TRAF3D Outlet
CFX Outlet
TRAF3D Inlet
Non-dimensional Span
Axial Velocity (m/s)
0
0.2
0.4
0.6
0.8
1
2
4
6
8
10

Figure 30

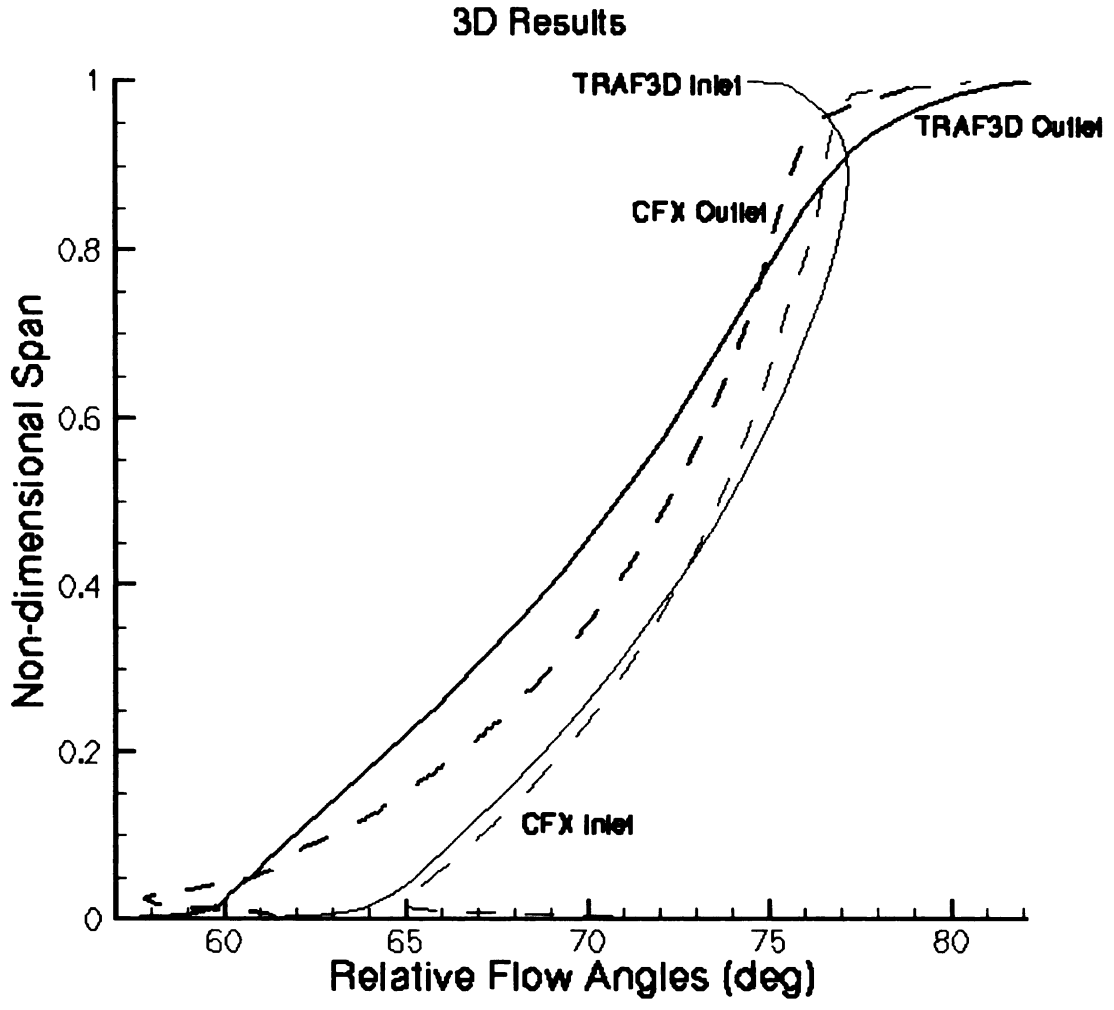

Figure 31

Another parameter worth noting is the radial velocity component. While no radial velocity was taken into account in the 1-D design, there is, never-the-less a very small radial component resulting from the TRAF3D calculation. While this component is probably too small to have a significant effect on the performance of the design, it should at least be noted that it is present and that the assumption used in the 1-D design that it is non-existent is not completely correct. The radial velocity distributions can be seen in Figure 32. The highest negative radial velocities can be found close to the mid-section of the blade. In addition, there is an increase toward hub and tip of the highest velocities.

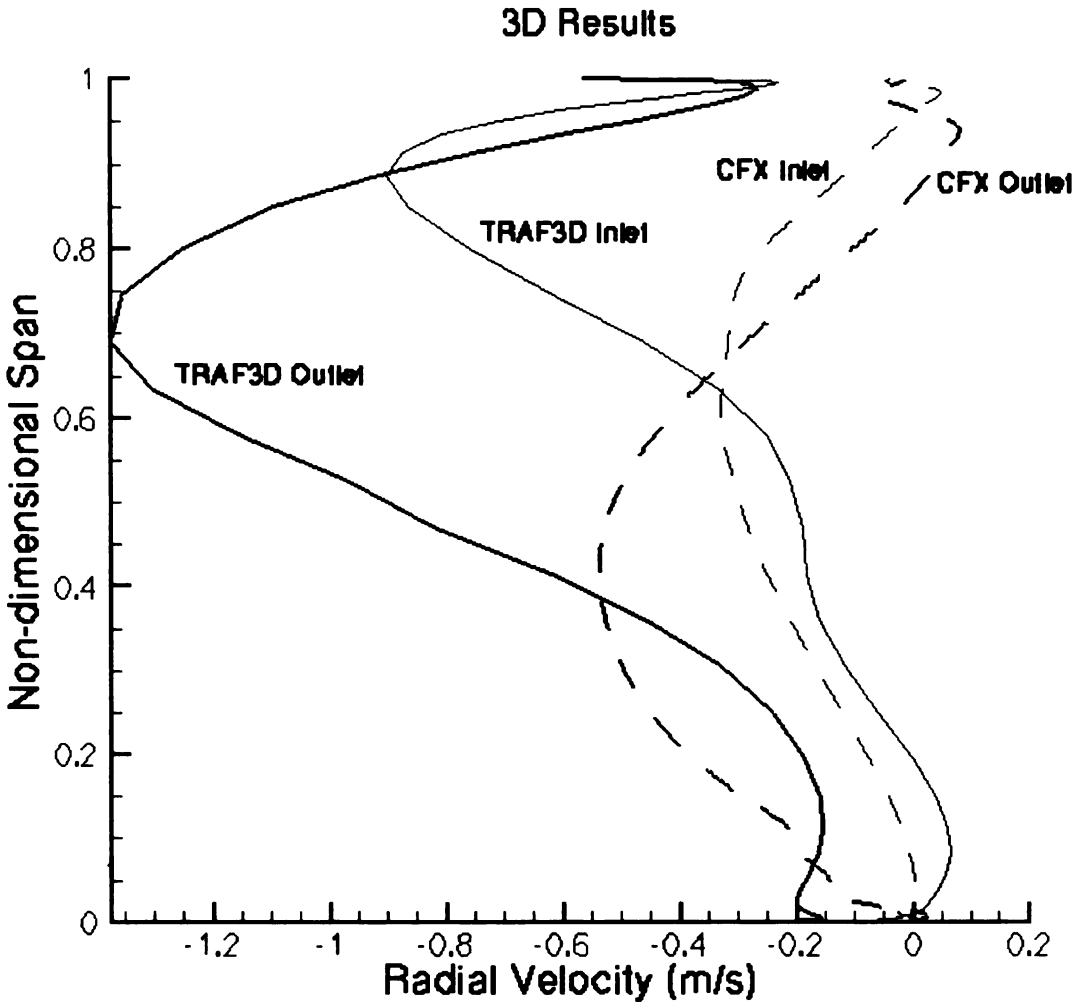

Figure 32

Blade-to-blade mach number plots are shown in Figures 34-38. There is a good visualization of the acceleration on the suction side, deceleration on the pressure side, and stagnation points at leading and trailing edges. The relative velocity vectors also follow the blades well at each section for both solvers. The vectors are less tangent to the leading edge for the TRAF3D solution than the CFX solution, again because of the longer rotating inlet used in the TRAF3D computations.

A performance map was created using the TRAF3D solver by imposing different static outlet pressures on the blade. The efficiency, mass flow rate, and pressure rise are plotted in Figure 39.

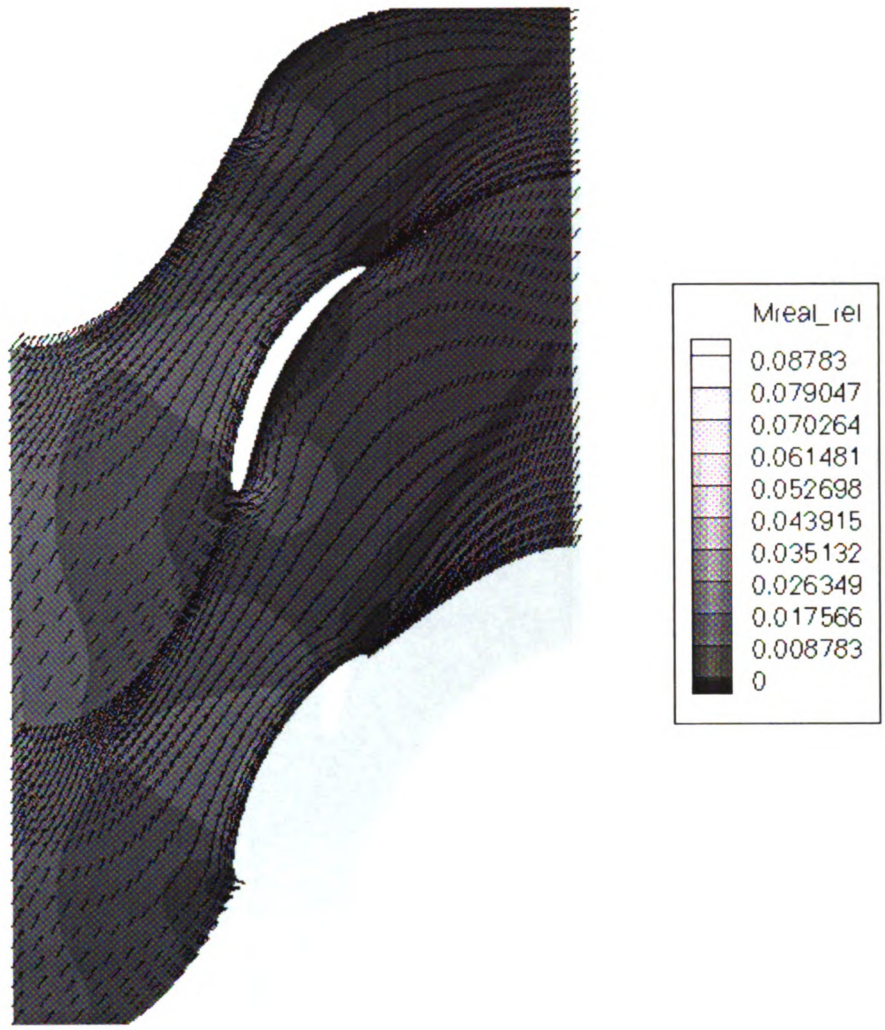
Mreal_rel
0.08783
0.079047
0.070264
0.061481
0.052698
0.043915
0.035132
0.026349
0.017566
0.008783
0

Figure 33

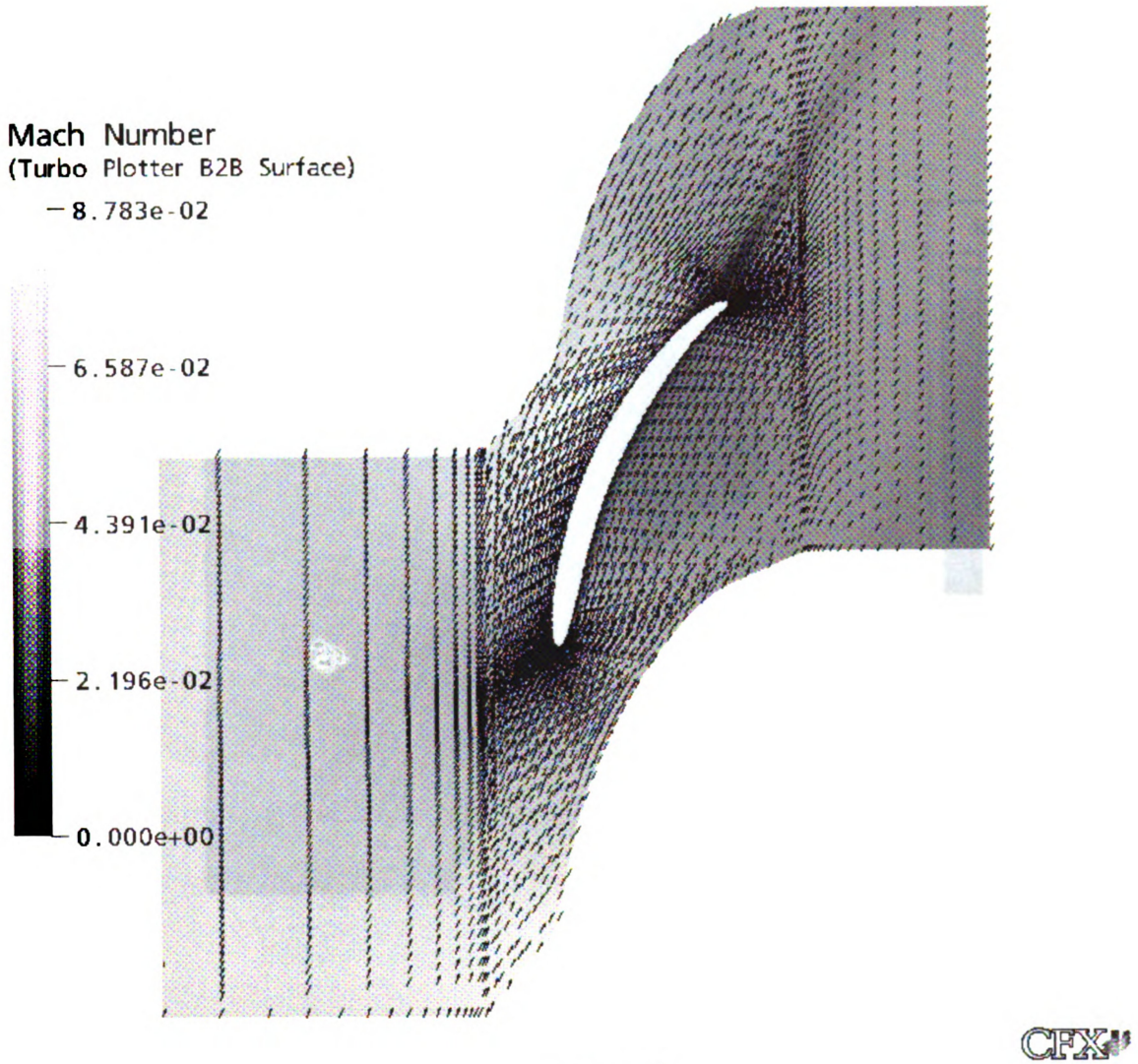
Mach Number
(Turbo Plotter B2B Surface)
8.783e-02
6.587e-02
4.391e-02
2.196e-02
0.000e+00
CFX

Figure 34

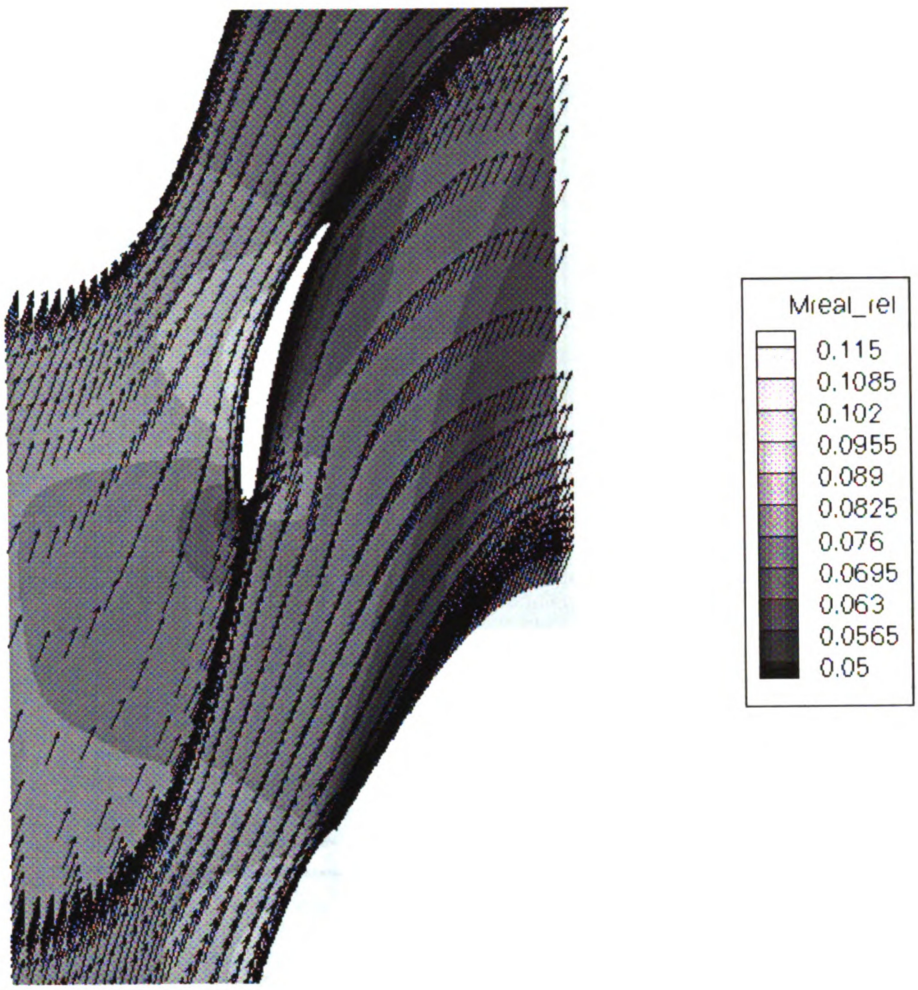
Mreal_rel
0.115
0.1085
0.102
0.0955
0.089
0.0825
0.076
0.0695
0.063
0.0565
0.05

Figure 35

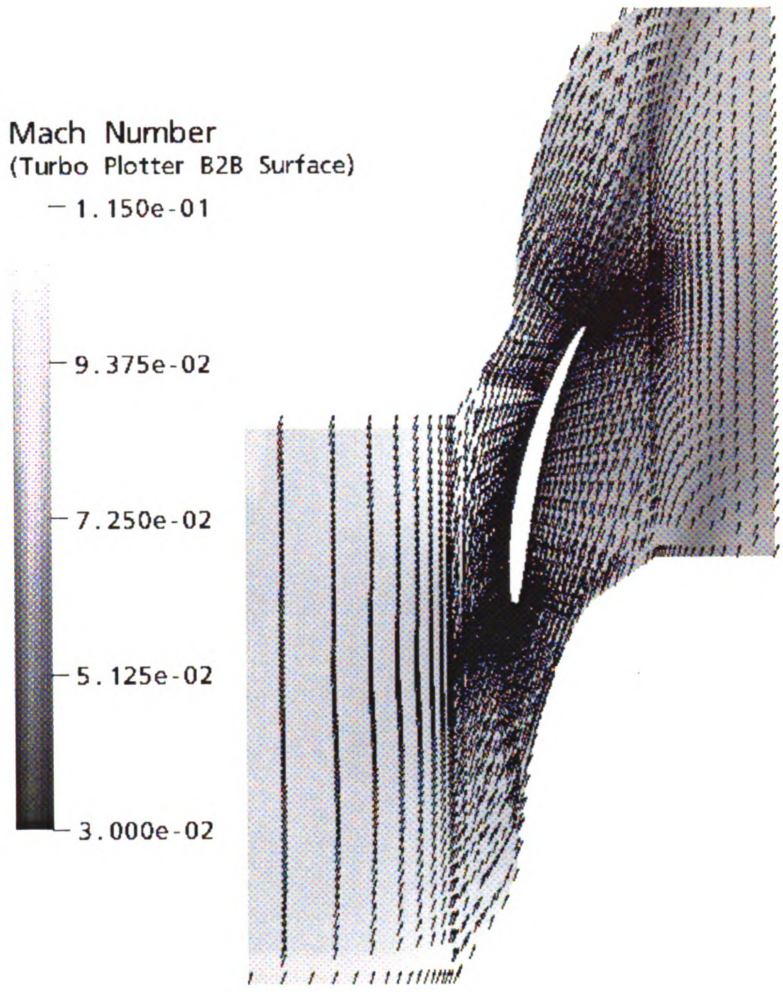
Mach Number
(Turbo Plotter B2B Surface)
1.150e-01
9.375e-02
7.250e-02
5.125e-02
3.000e-02

Figure 36

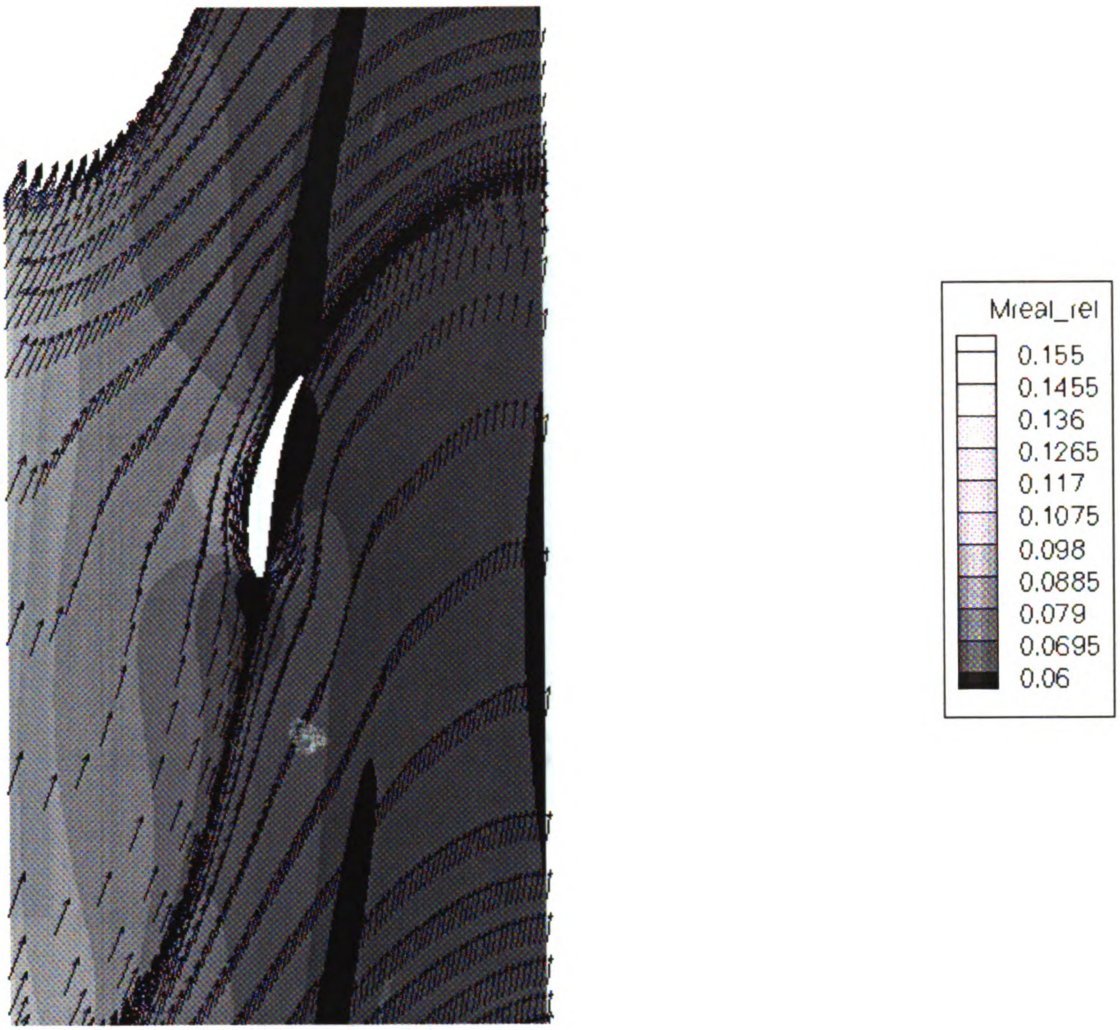
Mreal_rel
0.155
0.1455
0.136
0.1265
0.117
0.1075
0.098
0.0885
0.079
0.0695
0.06

Figure 37

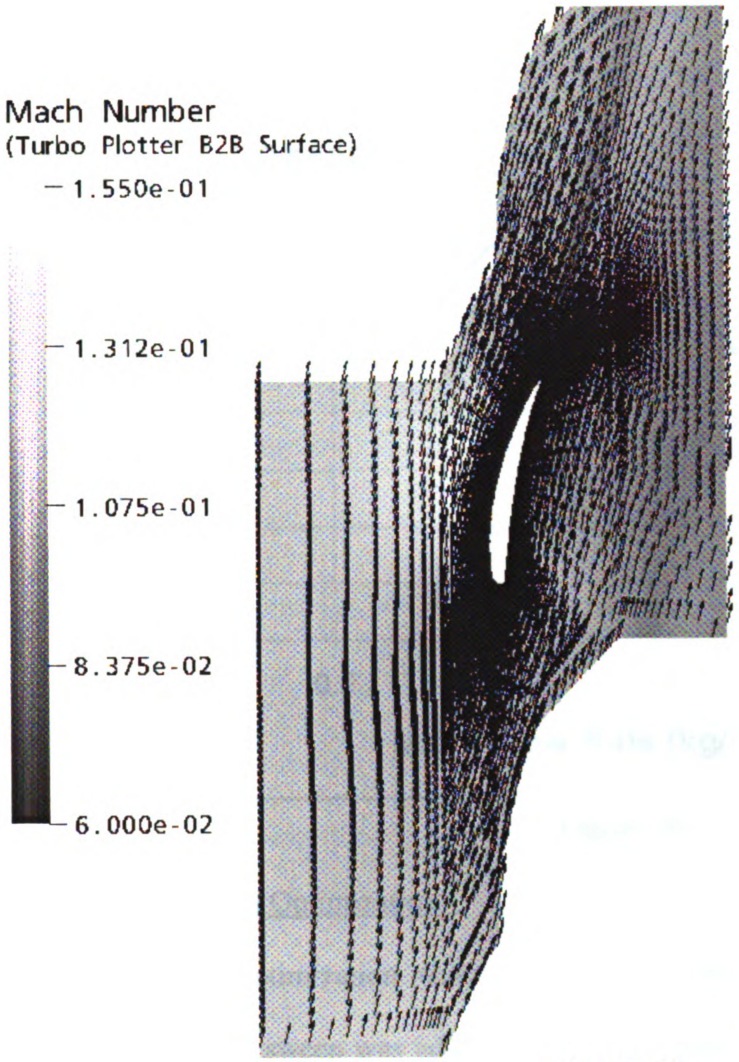
Mach Number
(Turbo Plotter B2B Surface)
1.550e-01
1.312e-01
1.075e-01
8.375e-02
6.000e-02

Figure 38

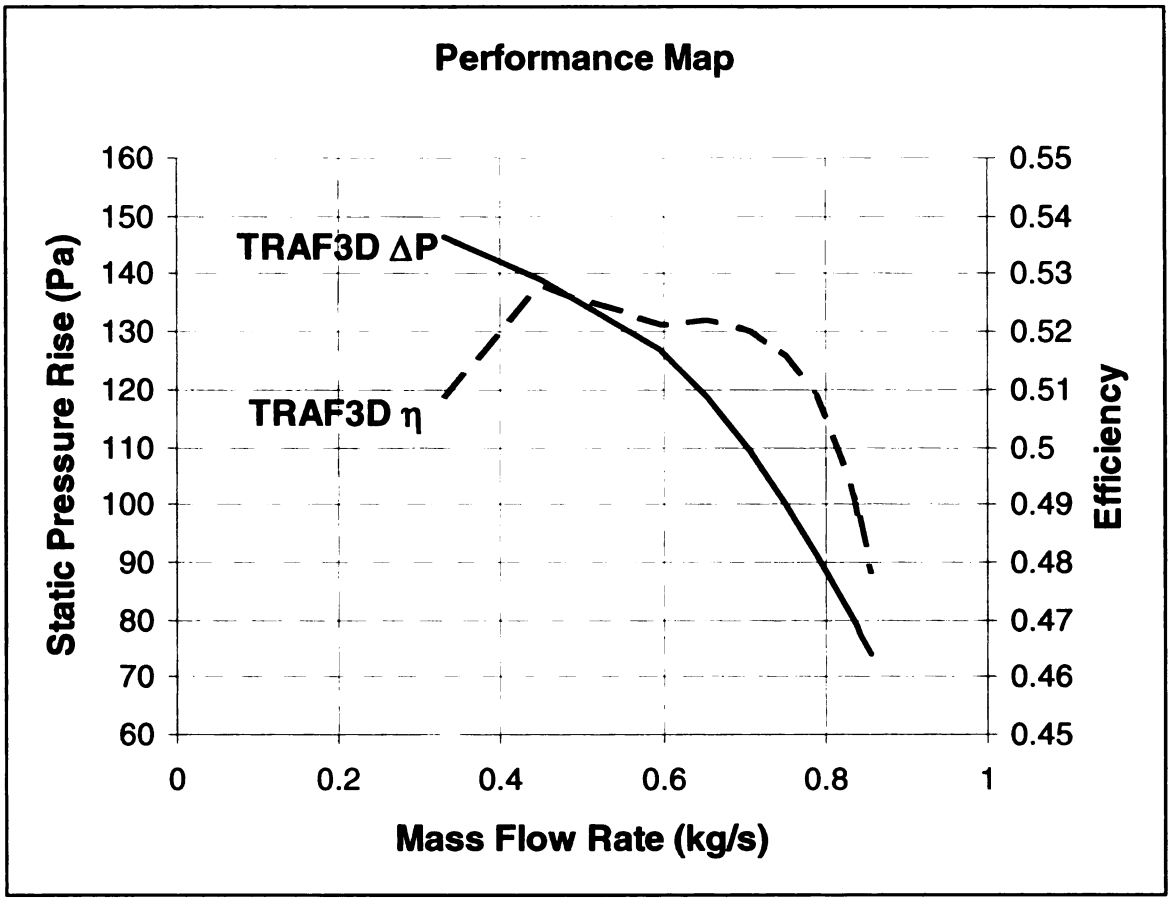

Figure 39

4.3.4 3-Dimensional Optimization

The 3-D Optimization was performed by adding lean in the circumferential direction. No axial sweep was added to the blades since that would extend the blade in the axial direction and require more space in the engine compartment. Eleven blade sections over the span and a new TRAF3D mesh were generated for the optimization to provide a smoothly curved blade. The hub section and next two radial sections were stacked radially, and then a circular arc was defined from the center of mass of the third section to a set circumferential location of the tip section center of mass. The center of mass of each of the intermediate sections fell on the arc. By increasing circumferential component of tip lean in the direction normal to the pressure side, the goal is to force the

work done by the middle and hub sections to increase while decreasing the work done by the tip section. In this way, the least efficient part of the blade would do the least amount of work. An example of a blade with a tip lean of 0.09 meters is shown in Figure 40. The efficiencies tend to increase with tip lean, as is shown across the span for several lean conditions in Figure 41. The efficiency increases with lean, especially near the tip section. The drop in efficiency at approximately 25% of the blade span corresponds to the place on the blade where the stacking changes from radial to leaned. The acute angle formed on the pressure side becomes more acute with increasing lean, and acute angles become sources of losses during stacking[4]. The blade turning, decreases near the tip with increasing lean (Figure 42) while turning increases near the hub section in accordance with predictions from a past Von Karman Institute lecture series[4]. The comparison of Figures 41 and 42 confirm that increasing the lean optimizes the performance of the blade. While the blade turning actually decreases near the tip with increasing lean, the efficiency near the tip actually increases due to the flow work being redistributed toward more efficient parts of the blade.

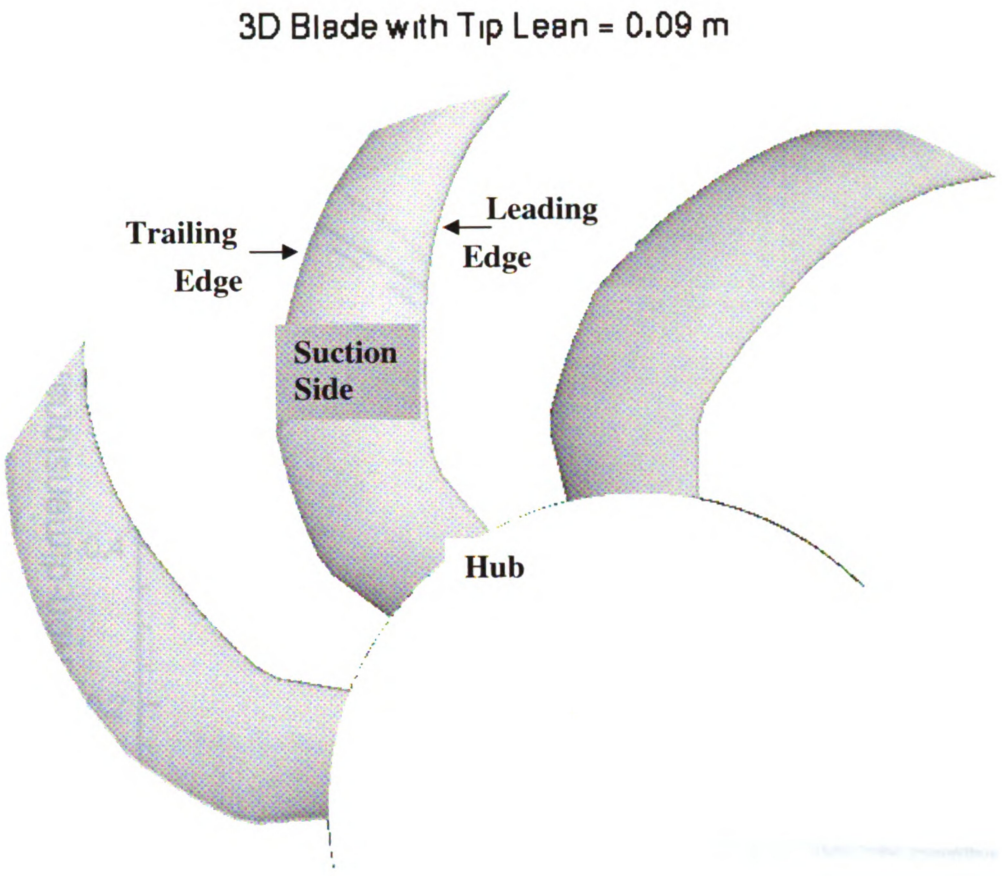
3D Blade with Tip Lean = 0.09 m
Trailing
Edge
Leading
Edge
Suction
Side
Hub

Figure 40

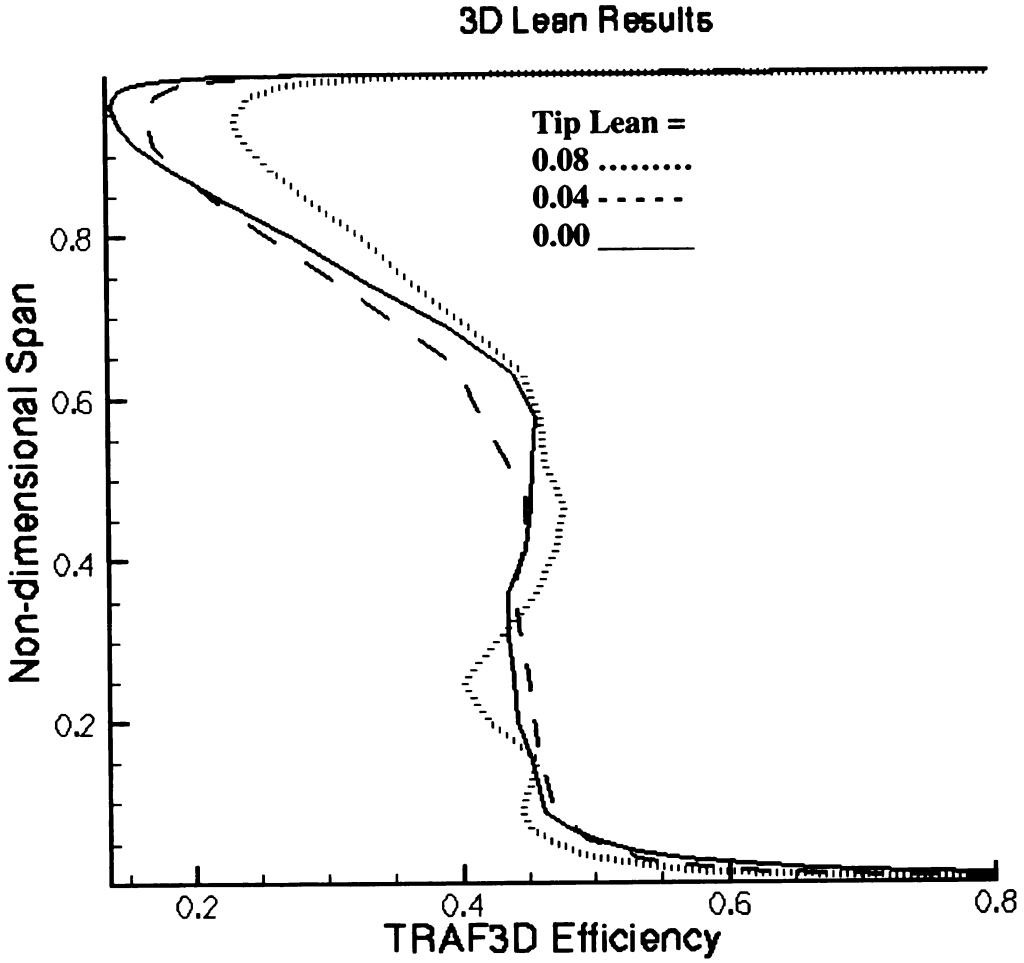
3D Lean Results
Tip Lean =
0.08 .....
0.04 - - - - -
0.00 _____
Non-dimensional Span
0.2
0.4
0.6
0.8
0.2
0.4
0.6
0.8
TRAF3D Efficiency

Figure 41

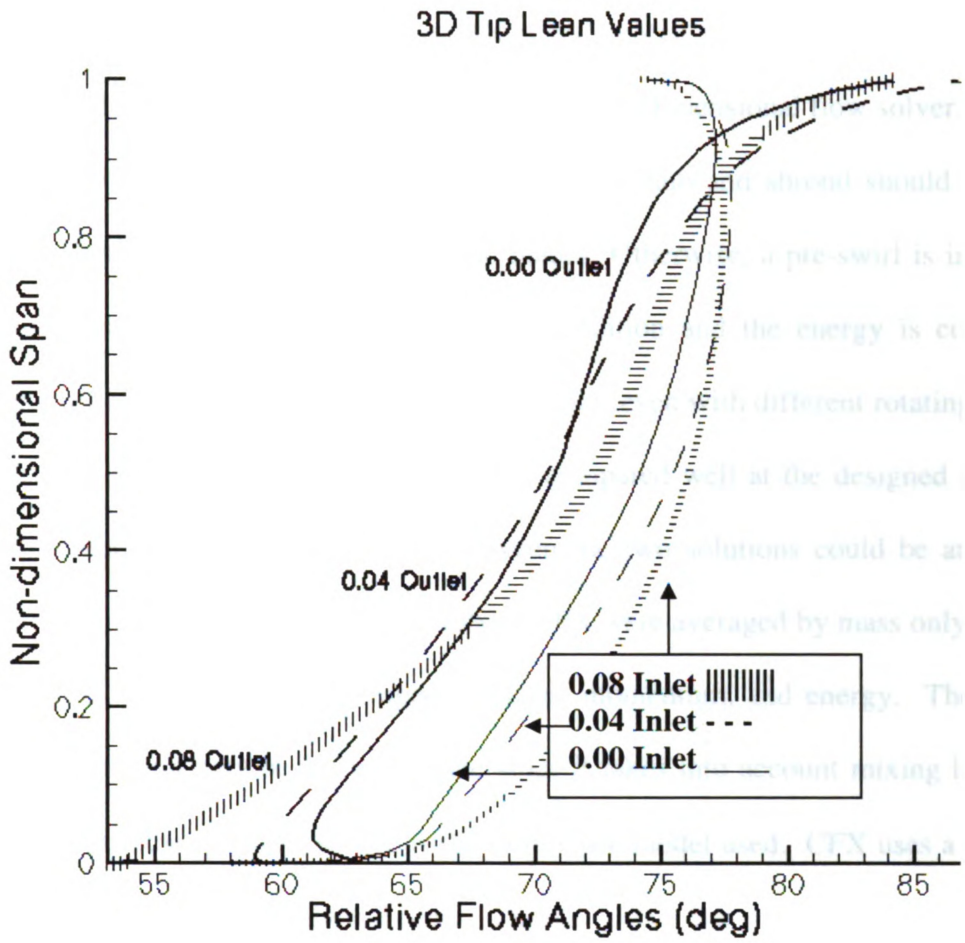

Figure 42

4.4 Conclusions

An axial cooling fan was designed for application in an automobile heat exchanging system. From the inlet conditions and constraints an initial 1-Dimensional design was performed, yielding flow angles for the blades and important initial thermodynamic values. 2-Dimensional blade sections were then designed using an inverse, inviscid method. The 2-Dimensional sections were then analyzed with a Navier-Stokes flow solver for comparison to the inviscid designs. The sections were then stacked and analyzed using two different 3-Dimensional Navier-Stokes solvers, and the

results were compared. Finally, several circumferential lean values were added to the stacking and the blades were again analyzed with a 3-Dimensional flow solver.

For highest efficiency and pressure rise, the hub and shroud should not extend much farther than the leading edge of the blades. Otherwise, a pre-swirl is imparted on the flow near the walls due to the no-slip condition and the energy is converted to temperature rise instead of pressure rise. However, even with different rotating inlet wall lengths, the results from TRAF3D and CFX compared well at the designed mass flow. The difference in static pressure rise between the two solutions could be attributed to several possible sources. First, the results of CFX were averaged by mass only, while the results from TRAF3D were averaged by mass, momentum, and energy. Therefore the TRAF3D solution may be more accurate since it takes into account mixing losses from the wake. Another possible source is the turbulence model used. CFX uses a k-ω model while TRAF3D uses a Baldwin-Lomax scheme. Also, the mesh quality can affect all results. A less-than-optimum grid for either solver could produce errors in the results.

Adding circumferential lean to the blade increases the overall efficiency of the blade but generally decreases the static pressure rise and mass flow rate. The reason for the increase in efficiency is that lean increases the work done by the most efficient parts of the blade (near the middle where endwall losses are low) and decreases the work done by the lesser efficient parts of the blade. A decrease in efficiency is observed at the location on the span where the stacking changes from radial to leaned, due to an accumulation of losses in the acute angle formed there on the pressure side. Using a completely leaned blade (without any radial stacking) could eliminate this zone of low efficiency, and would be a good candidate for future work.

APPENDICES

Appendix 5a

----------TRAF3D Results----------

MASS Averaged values for section : 1

---

mass flow = 0.840431333
mach averaged = 2.72347685E-02
ro averaged = 0.897607207
vx averaged = 10.4376307
vt averaged = -0.487607330
vr averaged = -0.366480708
Speed averaged = 10.4554386
vxr averaged = 10.4376307

vtr averaged = 37.1336327
vrr averaged = -0.366480708
p averaged = 101277.773
pe averaged = 101277.938
pt averaged = 101332.500
ptr averaged = 101977.234
pte averaged = 101332.523
t averaged = 393.140564
tt averaged = 393.201324
e averaged = 282139.000
alfa averaged = -2.32546568
delta averaged= -2.01091361
beta averaged = 74.3002319
vx(real) averaged (total
mass/(rho_av*tot_area))= 9.99389458

MASS Averaged values based on conservation of mass,
tangential and radial momentum and total energy (see VKI CN 141/TU)
VALUES after 3 iterations!

Paver = 101281.617 (Pa)
Poaver = 101326.633 (Pa)
Roaver = 0.897612512 (kg/m^3)

Alpha = -3.55518794 (deg)
Vmaver = 9.99383450 (m/s)
Vuaver = -0.620911360 (m/s)
Taver = 393.151398 (K)
Ttaver = 393.201324 (K)

MASS Averaged values for section : 2

---

mass flow = 0.835089684
mach averaged = 3.06479130E-02
ro averaged = 0.897414207
vx averaged = 10.2742290
vt averaged = -5.46047258
vr averaged = -0.770395339
Speed averaged = 11.6606188
vxr averaged = 10.2742290
vtr averaged = 31.8020630
vrr averaged = -0.770395339
p averaged = 101356.117
pe averaged = 101355.828
pt averaged = 101423.719
ptr averaged = 101885.602
pte averaged = 101423.320
t averaged = 393.529510
tt averaged = 393.604218
e averaged = 282433.312
alfa averaged = -26.8656254
delta averaged= -4.28820038
beta averaged = 72.0960083
vx(real) averaged (total mass/(rho_av*tot_area))= 9.99052143
Re2 aver.(based on Lref)= 9041.45020
Re2 aver.(based on chord)= 21946.2656

MASS Averaged values based on conservation of mass,
tangential and radial momentum
and total energy (see VKI CN 141/TU)
VALUES after 3 iterations!

Paver = 101356.250 (Pa)
Poaver = 101415.289 (Pa)
Roaver = 0.897389829 (kg/m^3)

Alpha = -29.4281540 (deg)
Vmaver = 9.99079323 (m/s)
Vuaver = -5.63598680 (m/s)
Taver = 393.538757 (K)
Ttaver = 393.604218 (K)
mass flow error = -6.35580812E-03
tot. press. rat. = 1.00089598
efficiency = 0.487949

Appendix 5b

----------CFX Results--------

--Mass Averaged Values at position 1--

rho1 = 0.897656 kg*m-3
Mrel1 = 0.0988336
M1 = 0.0275811
P1 = 101268 Pa
T1 = 392.942 K
Vax1 = 10.6613 m*s-1
Uave1 = 37.6941 m*s-1
Vrad1 = 0.186534 m*s-1
Vtan1 = -0.08334 m*s-1

--Mass Averaged Values at position 2--

rho1 = 0.898800 kg*m-3
Mrel1 = 0.0872737
M1 = 0.0288309
P1 = 101386 Pa
T1 = 393.116 K
Vax1 = 10.1308 m*s-1
Uave1 = 33.0955 m*s-1
Vrad1 = 0.268073 m*s-1
Vtan1 = -4.94675 m*s-1

efficiency = 0.772147

Appendix 5c

---------Equations----------

Velocity Trigonometry:

$$V = U + W \tag{1}$$

$$U = r * \omega \tag{2}$$

$$V_{ax} = V * \cos(\alpha) \tag{3}$$

$$V_{tan} = V * \sin(\alpha) \tag{4}$$

$$W_{ax} = W * \cos(\beta) \tag{5}$$

$$W_{tan} = W * \sin(\beta) \tag{6}$$

Blade Geometry:

$$r_{tip} = U_{tip} / (2*\pi*\omega/60) \tag{7}$$

$$r_{hub} = [r_{tip} - m / (\rho*\pi*V_{1,ax})]^{1/2} \tag{8}$$

$$t = (2*\pi*r) / Z \tag{9}$$

$$c_{ax} = c * \cos(\lambda) \tag{10}$$

Thermodynamics:

$$\Delta H = U * \Delta V_{tan} = U * V_{ax} * (\beta_2 - \beta_1) \tag{11}$$

$$\Delta P = \Delta H * \rho \tag{12}$$

$$\eta = (\Delta P/\rho) / (U * \Delta V_{tan}) \tag{13}$$

Coordinate Transformation:

$$x_{CFX} = x_{TRAF} \tag{14}$$

$$f = y_{\mathbf{TRAF}} / r \tag{15}$$

$$y_{\mathbf{CFX}} = r * \mathrm{Sin}(f) \tag{16}$$

$$z_{\mathbf{CFX}} = r * \mathrm{Cos}(f) \tag{17}$$

Table 1 Required Data

ω (rpm) =	2500	c_{hub} (m) =	0.04
U_{tip} (m/s) =	50	c_{mid} (m) =	0.05
T_{01} (K) =	393.15	c_{tip} (m) =	0.04
P_{01} (Pa) =	101300	V_1 (m/s) =	7.72145
λ_{hub} (deg) =	60.8	α_1 (deg) =	0
λ_{mid} (deg) =	75.3	m (kg/s) =	0.84
λ_{tip} (deg) =	78.5	ΔP (Pa) =	215
Z =	9		

Table 2 Values for Constant ΔP

r (m)	U (m/s)	$\Delta\beta$ (deg)	ΔP (Pa)
0.190985932	50	1.084448404	215
0.136499886	35.73559	3.560140908	215
0.082013841	21.47117	70.22043191	187.816

Table 3 Values for Actual Blade

r (m)	U (m/s)	$\Delta\beta$ (deg)	ΔP (Pa)
0.190985932	50	1.848218104	328.5753
0.136499886	35.73559	4.477440272	249.3758
0.082013841	21.47117	21.49543191	156.2893

REFERENCES

[1]Pehlivan, K. K., "Inverse Design and Optimization of an Axial Cooling Blower," Von Karman Institute Stagiere Report 2000-25. August 2000.

[2]Foss, J., Henner, M., Moreau, S., Neal, D., "Evaluating CFD Models of Axial Fans by Comparisons with Phase-Averaged Exeriments," SAE 2001, 01VTMS-89.

[3]Van den Braembussche, R. A., "Inverse Design Methods for Axial and Radial Turbomachines," Von Karman Institute Preprint 1994-35, May 1994.

[4]VKI LS 1999-02, "The Exploitation of 3-Dimensional Flow in Turbomachinery Design," *Turbomachinery Blade Design Systems*, Von Karman Institute 1999.